Studying models of balancing selection using phase-type theory

Kai Zeng[*,1], **Brian Charlesworth**[†] **and Asger Hobolth**[‡]

[*]Department of Animal and Plant Sciences, University of Sheffield, Sheffield S10 2TN, United Kingdom, [†]Institute of Evolutionary Biology, School of Biological Sciences, University of Edinburgh, Edinburgh EH9 3FL, United Kingdom, [‡]Department of Mathematics, Aarhus University, DK-8000 Aarhus C, Denmark

ABSTRACT Balancing selection is an important process, which maintains genetic variability in many functionally important genes. To increase our understanding of its effects on patterns of genetic diversity, we analyse two models of long-term balancing selection at a biallelic locus, one with a constant population size and the other with recent population size changes, as well as a model of recent balancing selection. We use time-inhomogeneous phase-type theory to obtain the expected properties of the gene tree at a neutral site linked to the target of selection, and the linkage disequilibrium (LD) between the selected and neutral sites. For long-term balancing selection, we show that selection targets with equilibrium allele frequencies close to 50% are easier to detect than targets with unequal allele frequencies. The target is also easier to identify after a population size reduction. The spread of a new mutation under balancing selection initially produces diversity patterns in linked neutral regions that are similar to those for a selective sweep caused by positive selection, including reduced diversity and an excess of both high and low frequency derived variants, as well as excess LD with the selected locus. Although the effects of recent balancing selection are more subtle, patterns of diversity and LD remain in a non-equilibrium state for a much longer period than with a sweep, and provide complementary information regarding the selection event. These results can be used for developing new methods for detecting loci under balancing selection, and illustrate the power of time-inhomogeneous phase-type theory, which can be applied to a wide range of population genetic problems.

KEYWORDS balancing selection; phase-type theory; demographic changes; linkage disequilibrium; site frequency spectrum; selective sweep

Balancing selection refers to a type of natural selection that maintains genetic variability in populations (Fisher 1922; Charlesworth 2006; Fijarczyk and Babik 2015). Genes known to be under balancing selection are often involved in important biological functions. Examples include the major histocompatibility complex (MHC) genes in vertebrates (Spurgin and Richardson 2010), plant self-incompatibility genes (Castric and Vekemans 2004), mating-type genes in fungi (van Diepen *et al.* 2013), genes underlying host-pathogen interactions (Bakker *et al.* 2006; Hedrick 2011), inversion polymorphisms (Dobzhansky 1970), and genes underlying phenotypic polymorphisms in many different organisms (e.g., Johnston *et al.* 2013; Kupper *et al.* 2016; Kim *et al.* 2019). More recently, it has been proposed that a related process, known as associative overdominance, may play a significant role in shaping diversity patterns in genomic regions with very low recombination rates (Becher *et al.* 2020; Gilbert *et al.* 2020). These facts highlight the importance of studying balancing selection.

Understanding how balancing selection affects patterns of genetic variability is a prerequisite for detecting genes under this type of selection. The best studied models involve long-term selection acting at a single locus (Strobeck 1983; Hudson and Kaplan 1988; Takahata 1990; Takahata and Nei 1990; Vekemans and Slatkin 1994; Nordborg 1997; Takahata and Satta 1998; Innan and Nordborg 2003). It is well known that, in addition to maintaining diversity at the selected locus, long-term balancing selection increases diversity at closely linked neutral sites. This reflects an increased coalescence time for the gene tree connecting the alleles in a sample from the current population. When this tree is sufficiently deep, it is possible for the ages of the alleles to exceed the species' age, leading to trans-species polymorphism. Furthermore, long-term balancing selection alters the site frequency spectrum (SFS) at linked neutral sites, causing

doi: 10.1534/genetics.XXX.XXXXXX
Manuscript compiled: Monday 6th July, 2020
[1]Corresponding author: Department of Animal and Plant Sciences, University of Sheffield, Sheffield S10 2TN, United Kingdom. Email: k.zeng@sheffield.ac.uk.

an excess of intermediate frequency derived variants. These properties underlie most of the methods used for scanning large-scale genomic data for targets of balancing selection (Andres *et al.* 2009; Leffler *et al.* 2013; DeGiorgio *et al.* 2014; Bitarello *et al.* 2018; Cheng and DeGiorgio 2019; Siewert and Voight 2020).

Most previous studies have assumed that the population is at statistical equilibrium under selection, mutation and genetic drift, which is a serious limitation. In reality, most populations have experienced recent changes in population size. There is currently no effective way to make predictions about the joint effects of demographic changes and balancing selection on patterns of genetic variability in nearby regions, which limits our ability to construct methods for analysing data from these populations. Moreover, many cases of balancing selection involve variants that have only recently spread to intermediate frequencies, rather than having been maintained for periods much greater than the neutral coalescent time (e.g. Eanes 1999; Kwiatkowski 2005; Corbett-Detig and Hartl 2012). Indeed, recent theoretical studies have suggested that adaptation may occur through the frequent emergence of short-lived balanced polymorphism (Sellis *et al.* 2011; Connallon and Clark 2014). Because of their young age, the characteristic diversity patterns predicted for long-term balancing selection may not be generated. As a result, targets of such selection are unlikely to be detected by existing genome scan methods. This is consistent with the relatively small number of potential targets returned by genome scans (Andres *et al.* 2009; Leffler *et al.* 2013; DeGiorgio *et al.* 2014; Bitarello *et al.* 2018; Cheng and DeGiorgio 2019).

Multiple authors have suggested that the emergence of recent balanced polymorphism will generate diversity patterns that resemble those generated by incomplete selective sweeps (Charlesworth 2006; Sellis *et al.* 2011; Fijarczyk and Babik 2015), and methods designed for detecting sweeps can indeed pick up these signals (e.g., Zeng *et al.* 2006). However, there is currently no theoretical framework for studying recent balanced polymorphism and quantifying its effects on diversity patterns in nearby regions, which precludes a detailed comparison with incomplete selective sweeps. Acquiring this knowledge will help us devise methods for distinguishing between these two forms of selection, which will in turn help us to test hypotheses about the role of balancing selection in adaptation.

Here we tackle these problems by developing and applying time-inhomogeneous phase-type theory, thus extending a recent study in which a time-homogeneous version of the theory was used to study several population genetic models at statistical equilibrium (Hobolth *et al.* 2019). This method is essentially an extension of the backwards matrix representation of the structured coalescent process that has previously been applied to the analysis of the effects of balancing selection on a linked neutral site (Nordborg 1997). We prove several useful results under the time-inhomogeneous framework, and use them to analyse three models of balancing selection: an equilibrium model of long-term balancing selection, a model with strong, long-term balancing selection and changes in population size, and a model with recent balancing selection. The analysis of the last model is accompanied by a comparison with a comparable selective sweep model.

For each of these models, we obtain four statistics that are useful for understanding the effects of selection on diversity patterns in neutral regions linked to the target of selection. For a sample of alleles collected from a neutral site, we calculate (1) the expected pairwise coalescence time, (2) the expected level of linkage disequilibrium (LD) between the selected locus and the focal neutral site, (3) the total branch length of the gene tree, and (4) the site frequency spectrum (SFS). Our results extend previous studies of the equilibrium model by providing a unifying framework for obtaining these statistics. The analysis of the non-equilibrium models provides useful insights that can be used for devising new genome scan methods or parameter estimation methods. We conclude the study by discussing the usefulness of phase-type theory in population genetics.

An equilibrium model of balancing selection

Consider a diploid, randomly mating population. The effective population size N_e is assumed to be constant over time. An autosomal locus with two alleles A_1 and A_2 is under balancing selection. The intensity of selection is assumed to be sufficiently strong and constant over time that the frequencies of the two alleles remain at their equilibrium values indefinitely. Denote the equilibrium frequencies of A_1 and A_2 by $\hat{p}_1$ and $\hat{p}_2$, respectively ($\hat{p}_1 + \hat{p}_2 = 1$). Note that this set-up can accommodate any model of long-term balancing selection (with or without reversible mutation between A_1 and A_2), as long as it produces these equilibrium allele frequencies. Consider a sample of n alleles with respect to a linked neutral locus, with a recombination frequency r with the selected locus. In the following four subsections, we use time-homogeneous phase-type theory to calculate the four statistics mentioned at the end of the Introduction. This introduces the methodology and notation, and sets the stage for extending the analysis to non-equilibrium models in later sections. A similar model has been investigated previously using different approaches (Strobeck 1983; Hudson and Kaplan 1988; Nordborg 1997). However, these do not provide analytical expressions for the SFS.

The mean coalescence time for a sample size of two

Each of the two alleles in the sample is associated with either A_1 or A_2 at the selected site. The sample is therefore in one of three possible states (Figure 1). In state 1, both alleles are associated with A_2. In state 2, one allele is associated with A_1, and the other is associated with A_2. In state 3, both alleles are associated with A_1. Take state 1 as an example. An allele currently associated with A_2 was associated with A_1 in the previous generation either because there was an A_1 to A_2 mutation during gamete production, or because the parent was an A_1A_2 heterozygote and there was a recombination event. Define v_{21} as the (backward) mutation rate. The first event occurs with probability v_{21}, and the second event occurs with probability $r\hat{p}_1$. The probability that the focal allele becomes associated with A_1 in the previous generation is $m_{21} = v_{21} + r\hat{p}_1$. The two alleles in state 1 may share a common ancestor in the previous generation. Because the frequency of A_2 is $\hat{p}_2$, a total of $2N_e\hat{p}_2$ alleles were associated with A_2 in the previous generation. The chance that the two alleles coalesce is $1/(2N_e\hat{p}_2)$.

Under the standard assumption that the probability of occurrence of more than one event in one generation is negligible, the probability that the two alleles in state 1 remain unchanged for z generations is:

$$\left(1 - 2m_{21} - \frac{1}{2N_e\hat{p}_2}\right)^z \approx e^{-\left(2m_{21}+\frac{1}{2N_e\hat{p}_2}\right)z} = e^{-\left(2M_{21}+\frac{1}{\hat{p}_2}\right)t} \quad (1)$$

where $M_{21} = 2N_e m_{21} = \mu_{21} + \rho\hat{p}_1$, $\mu_{21} = 2N_e v_{21}$, $\rho = 2N_e r$, and $t = z/(2N_e)$.

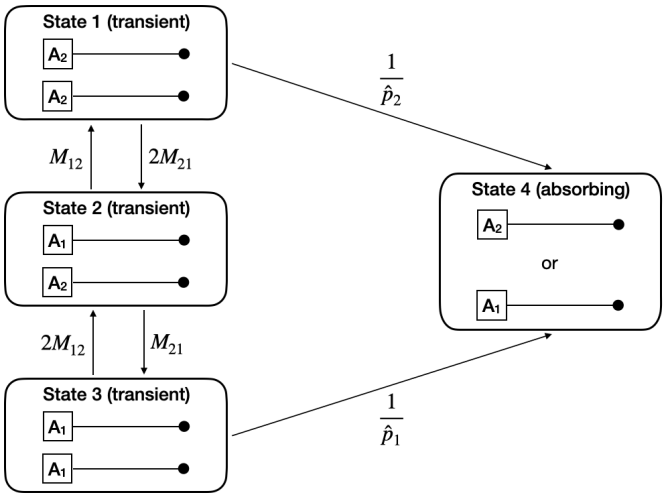

Figure 1 Transition rates between the states of the equilibrium balancing selection model for a sample size of two. Time is scaled in units of $2N_e$ generations. The equilibrium frequencies of A_1 and A_2 are $\hat{p}_1$ and $\hat{p}_2$, respectively. $M_{ij} = \mu_{ij} + \rho\hat{p}_j$, where $\mu_{ij} = 2N_e v_{ij}$ and $\rho = 2N_e r$. The neutral locus is represented by a black dot.

We have scaled time in units of $2N_e$ generations, and will use this convention throughout unless stated otherwise. Using this timescale, when in state 1, the waiting time to the next event follows an exponential distribution with rate parameter $2M_{21} + (1/\hat{p}_2)$. Given that an event has occurred, it is either caused by one of the two alleles becoming associated with A_1 with probability $2M_{21}/(2M_{21} + 1/\hat{p}_2)$, or by coalescence of the two alleles with probability $(1/\hat{p}_2)/(2M_{21} + 1/\hat{p}_2)$. As illustrated in Figure 1, the first possibility moves the process from state 1 to state 2, whereas the second possibility terminates the process by moving it into the absorbing state where the most recent common ancestor (MRCA) is reached (state 4).

We can derive the transition rates between all four states of the process using similar arguments (Figure 1). This model is analogous to a two-deme island model in which $2N_e\hat{p}_1$ and $2N_e\hat{p}_2$ are the sizes of the two demes, and M_{12} and M_{21} are scaled (backward) migration rates (e.g., Slatkin 1991; Nordborg 1997). Hereafter, we refer to the sub-population consisting of alleles associated with A_1 or A_2 as allelic class 1 or 2, respectively.

We can analyse this model efficiently using time-homogeneous phase-type theory (Hobolth *et al.* 2019). To this end, we define an intensity (rate) matrix as:

$$\boldsymbol{\Lambda} = \begin{bmatrix} -2M_{21} - \frac{1}{\hat{p}_2} & 2M_{21} & 0 & \frac{1}{\hat{p}_2} \\ M_{12} & -M_{12} - M_{21} & M_{21} & 0 \\ 0 & 2M_{12} & -2M_{12} - \frac{1}{\hat{p}_1} & \frac{1}{\hat{p}_1} \\ 0 & 0 & 0 & 0 \end{bmatrix}. \quad (2)$$

The first three rows in $\boldsymbol{\Lambda}$ are for states 1, 2, and 3, respectively. In row i ($i \in \{1,2,3\}$), the $j-$th element is the rate of jumping from state i to state j ($j \neq i$ and $j \in \{1,2,3,4\}$), and the diagonal element is the negative of the sum of all the other elements in this row. All elements of the last row of $\boldsymbol{\Lambda}$ are zero because state 4 is absorbing, so that the rate of leaving it is zero. Note that $\boldsymbol{\Lambda}\vec{1} = \vec{0}$, where $\vec{1}$ is a vector of ones and $\vec{0}$ is a vector of zeros.

We can write $\boldsymbol{\Lambda}$ in a more compact form:

$$\boldsymbol{\Lambda} = \begin{bmatrix} \boldsymbol{S} & \boldsymbol{s} \\ \vec{0} & 0 \end{bmatrix} \quad (3)$$

where $\boldsymbol{S}$ represents the 3-by-3 sub-matrix in the upper left corner of $\boldsymbol{\Lambda}$, and $\boldsymbol{s}^T = (\frac{1}{\hat{p}_2}, 0, \frac{1}{\hat{p}_1})$ consists of the first three elements in the last column of $\boldsymbol{\Lambda}$. Thus, $\boldsymbol{S}$ contains the transition rates between the transient states, and $\boldsymbol{s}$ contains the rates of jumping to the absorbing state. $\boldsymbol{S}$ and $\boldsymbol{s}$ are referred to as the sub-intensity matrix and the exit rate vector, respectively.

Let $T_{i,2-i}$ be the expected time to the MRCA, given that i and $2-i$ alleles in the sample are associated with A_1 and A_2, respectively. Let the initial condition vector be $\boldsymbol{\alpha} = (\alpha_1, \alpha_2, \alpha_3)$, where α_i is the probability that the sample is in state i ($\sum_1^3 \alpha_i = 1$). For example, if the sample is in state 1, then $\boldsymbol{\alpha} = (1,0,0)$; using phase-type theory (Hobolth *et al.* 2019), we have:

$$T_{0,2} = \boldsymbol{\alpha}\boldsymbol{U}\vec{1} = \sum_{k=1}^{3} u_{1k} \quad (4)$$

where $\boldsymbol{U} = \{u_{ij}\} = -\boldsymbol{S}^{-1}$, and u_{ij} gives us the expected amount of time the process spends in state j prior to coalescence, provided that the initial state is i ($i, j \in \{1,2,3\}$).

$\boldsymbol{U}$ is referred to as the Green's matrix. By changing $\boldsymbol{\alpha}$, we can obtain all the $T_{i,2-i}$ without the need to recalculate $\boldsymbol{U}$. More generally, we can use phase-type theory to obtain the probability density function and all the moments of the coalescence time (Hobolth *et al.* 2019). It is possible to obtain $\boldsymbol{U}$ analytically for the general model with reversible mutation between A_1 and A_2, as specified by (2). However, its terms are complicated, and are not shown. For sites that are not very tightly linked to the selected locus, movements of lineages between the two allelic classes are primarily driven by recombination (i.e., $\rho \gg \mu_{ij}$).Furthermore, with only two alleles at the selected locus, the general model is most appropriate for cases where the selected locus contains a small handful of nucleotides. In this case μ_{ij} is of the order of the average nucleotide diversity at neutral sites (e.g., about 0.02 in *Drosophila melanogaster* or about 0.001 in humans).

For most applications, therefore, it is sufficient to work with a simplified model with $\mu_{ij} = 0$. In this case, we have $\hat{p}_1 M_{12} = \hat{p}_2 M_{21}$ (i.e., there is conservative migration; Nagylaki (1980)), which leads to:

$$\boldsymbol{U} = \begin{bmatrix} \frac{\hat{p}_2 + 2\hat{p}_1\hat{p}_2^3\rho}{1+2\hat{p}_1\hat{p}_2\rho} & 2\hat{p}_1\hat{p}_2 & \frac{2\hat{p}_1^3\hat{p}_2\rho}{1+2\hat{p}_1\hat{p}_2\rho} \\ \hat{p}_2^2 & 2\hat{p}_1\hat{p}_2 + \frac{1}{\rho} & \hat{p}_1^2 \\ \frac{2\hat{p}_1\hat{p}_2^3\rho}{1+2\hat{p}_1\hat{p}_2\rho} & 2\hat{p}_1\hat{p}_2 & \frac{\hat{p}_1 + 2\hat{p}_1^3\hat{p}_2\rho}{1+2\hat{p}_1\hat{p}_2\rho} \end{bmatrix}. \quad (5)$$

Summing the three rows, we have:

$$\begin{cases} T_{0,2} = 1 - \frac{\hat{p}_1(\hat{p}_1 - \hat{p}_2)}{1+2\hat{p}_1\hat{p}_2\rho} \\ T_{1,1} = 1 + \frac{1}{\rho} \\ T_{2,0} = 1 + \frac{(\hat{p}_1 - \hat{p}_2)\hat{p}_2}{1+2\hat{p}_1\hat{p}_2\rho} \end{cases} \quad (6)$$

These results are the same as those derived by Nordborg (1997). The additional insight obtained here is given by (5). For instance, regardless of whether the initial state is 1 or 3, the process spends, on average, an equal amount of time in state 2 before coalescence (i.e., $u_{12} = u_{32}$ in (5)). The results presented

in Figure S1 further confirm that the simplified model should suffice in most cases, because the general model converges quickly to the simplified model.

Let $\pi_{i,2-i}$ be the expected diversity when i and $2-i$ alleles in the sample are associated with A_1 and A_2, respectively. Under the infinite sites model (Kimura 1969), $\pi_{i,2-i} = 2\theta T_{i,2-i}$, where $\theta = 2N_e v$ and v is the mutation rate per generation at the neutral site. From (6), we can see that $T_{1,1}$ is independent of $\hat{p}_1$ and $\hat{p}_2$, and is always greater than 1, which is the expected coalescence time under the standard neutral model with constant population size. Note also that $T_{0,2}$ is < 1 or > 1 when $\hat{p}_2$ is < 0.5 or > 0.5. Similarly, $T_{2,0}$ is < 1 or > 1 when $\hat{p}_1$ is < 0.5 or > 0.5. These trends hold even when there is reversible mutation between A_1 and A_2 (Figure S1).

In reality, the selected variants are often unknown, and detection of targets of balancing selection typically relies on investigating how diversity levels change along the chromosome (Charlesworth 2006; Fijarczyk and Babik 2015). It is therefore useful to consider the expected coalescence time for two randomly sampled alleles at the neutral site, defined as:

$$T = \hat{p}_1^2 T_{2,0} + 2\hat{p}_1\hat{p}_2 T_{1,1} + \hat{p}_2^2 T_{0,2} = 1 + \frac{\hat{p}_1\hat{p}_2(\rho+2)}{\rho(1+2\hat{p}_1\hat{p}_2\rho)} \qquad (7)$$

where the results in (6) are used. The nucleotide site diversity is given by $\pi = 2T\theta$. Figure 2 shows that the diversity level is highest when $\hat{p}_1 = \hat{p}_2 = 0.5$. This is also true when there is reversible mutation between A_1 and A_2 (Figure S2). The simplified model is inherently symmetrical. For example, the curve for $\hat{p}_1 = 0.25$ is identical to that for $\hat{p}_1 = 0.75$. These results suggest that targets of balancing selection are easiest to detect when the equilibrium frequencies of the selected variants are close to 50%. In all cases, marked effects on diversity are only seen with ρ of order 1 or less.

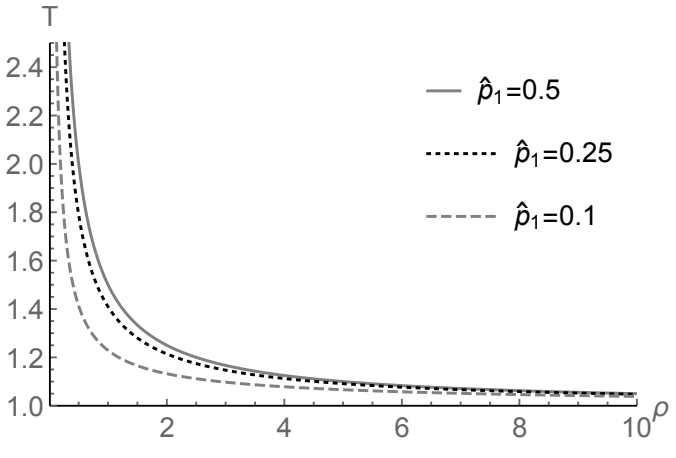

Figure 2 The expected pairwise coalescence time as a function of ρ. The simplified model with $\mu_{12} = \mu_{21} = 0$ is considered. $\hat{p}_1$ is the equilibrium frequency of A_1 at the selected locus.

LD between the selected locus and a linked neutral site

The expected pairwise coalescence time obtained in the previous section can be used to calculate a measure of LD between the two loci (Charlesworth *et al.* 1997). Assume that the neutral locus is segregating for two variants B_1 and B_2. Let the frequencies of B_1 in allelic class 1 and 2 be x and y, respectively. Thus, the frequency of B_1 in the population is $q_1 = \hat{p}_1 x + \hat{p}_2 y$, and that of B_2 is $q_2 = 1 - q_1$. Let $\delta = x - y$. The coefficient of LD between the two loci is given by $D = \hat{p}_1\hat{p}_2\delta$ (see Chap. 8 of Charlesworth and Charlesworth 2010, p. 410). The corresponding correlation coefficient is $R^2 = D^2/(\hat{p}_1\hat{p}_2 q_1 q_2)$. It is impossible to derive a simple expression for $\mathbb{E}[R^2]$. An alternative that has been widely used can be written as:

$$\sigma^2 = \frac{\mathbb{E}[D^2]}{\mathbb{E}[\hat{p}_1\hat{p}_2 q_1 q_2]} = \frac{\hat{p}_1^2\hat{p}_2^2\mathbb{E}[\delta^2]}{\hat{p}_1\hat{p}_2\mathbb{E}[q_1 q_2]} = \frac{\hat{p}_1\hat{p}_2\mathbb{E}[\delta^2]}{\mathbb{E}[q_1 q_2]} \qquad (8)$$

where we have used the fact that $\hat{p}_1$ and $\hat{p}_2$ are assumed to be constant (Ohta and Kimura 1971; Strobeck 1983; McVean 2002). Note that $\pi = 2\mathbb{E}[q_1 q_2]$ is the expected diversity at the neutral site.

As discussed in the previous section, we have $\pi = 2\theta T$ under the infinite sites model. To relate $E[\delta^2]$ to the expected pairwise coalescence times, we first define the expected diversity within allelic class 1 and allelic class 2 as $\pi_{A1} = 2\mathbb{E}[x(1-x)]$ and $\pi_{A2} = 2\mathbb{E}[y(1-y)]$, respectively. Again, under the infinite sites model, we have $\pi_{A1} = 2\theta T_{2,0}$ and $\pi_{A2} = 2\theta T_{0,2}$. In addition, let the weighted within allelic class diversity be $\pi_A = \hat{p}_1\pi_{A1} + \hat{p}_2\pi_{A2}$. Note that $\pi - \pi_A = 2\mathbb{E}[q_1 q_2 - \hat{p}_1 x(1-x) - \hat{p}_2 y(1-y)] = 2\hat{p}_1\hat{p}_2\mathbb{E}[\delta^2]$. Inserting these results into right-most term of (8), we have:

$$\sigma^2 = \frac{\pi - \pi_A}{\pi} = \frac{T - T_A}{T} \qquad (9)$$

where $T_A = \hat{p}_1 T_{2,0} + \hat{p}_2 T_{0,2}$ is the weighted average within allelic class coalescence time. Note that σ^2 has the same form as the fixation indices (e.g., F_{ST}) widely used in studies of structured populations. This close relationship between LD and the fixation indices was first pointed out by Charlesworth *et al.* (1997), who referred to σ^2 as F_{AT}. Our treatment here clarifies the relevant statements in this previous study. It also provides a genealogical interpretation of the results of Strobeck (1983).

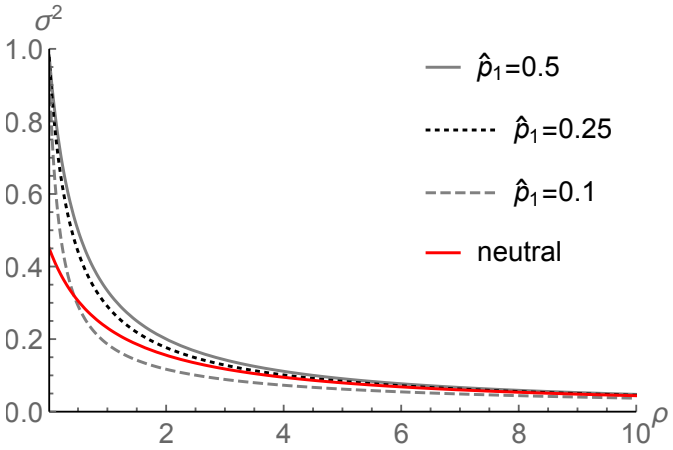

Figure 3 The level of LD between the selected and neutral loci as a function of ρ. The simplified model with $\mu_{12} = \mu_{21} = 0$ is considered. The neutral expectation for σ^2 is also included.

Figure 3 shows σ^2 as a function of ρ generated under the simplified model with $\mu_{12} = \mu_{21} = 0$. The level of LD between the selected and neutral loci is highest when $\hat{p}_1 = \hat{p}_2 = 0.5$, and decreases as $\hat{p}_1$ moves close to either 0 or 1 (note that the model is symmetrical such that, for $0 < z < 1$, the curve for $\hat{p}_1 = z$ is identical to that for $\hat{p}_1 = 1 - z$). As expected, reversible mutation between A_1 and A_2 lowers LD by increasing the rate at

which lineages move between the two allelic classes (Figure S3). These results mirror those described above for diversity levels. Together they show that the effect of balancing selection on linked diversity and LD patterns is largest when the equilibrium frequencies of the selected variants are close to 50%.

It is informative to compare LD patterns under balancing selection with those under neutrality (i.e., $\sigma^2 = (5+\rho)/(11+13\rho+2\rho^2)$; Ohta and Kimura 1971). With balancing selection and $\hat{p}_1 = 0.5$, elevated LD is observed when $\rho < 4$ (Figure 3). With $\hat{p}_1 = 0.1$, LD is higher than neutral expectation when $\rho < 0.5$, and it becomes lower than the neutral level when $\rho > 0.5$. Considering crossover alone, the scaled recombination rate per site is of the order of 0.002 in humans, and 0.02 in *Drosophila*. These values go up substantially if we also take into account gene conversion (e.g., Campos and Charlesworth 2019). Thus, even when the effect of balancing selection is at its maximum, the region affected is small. The effect becomes rather insubstantial when the equilibrium frequency is close to 0 or 1, suggesting that such selection targets are probably extremely difficult to detect.

Total branch length

We now consider the situation when a sample of n alleles is available, with n_1 of them associated with A_1 and n_2 with A_2 ($n_1 + n_2 = n$). Let L_{n_1,n_2} be the the expected total branch length of the gene tree that describes the ancestry of the sample with respect to a neutral site linked to the selected locus. Under the infinite sites model, the expected number of segregating sites in the sample is given by $\theta L_{n_1,n_2}$. Thus, L_{n_1,n_2} is closely related to Watterson's θ_W (Watterson 1975) and Tajima's D (Tajima 1989), both of which are frequently used in the search for selection targets (Charlesworth 2006; Fijarczyk and Babik 2015). There are also other ways in which L_{n_1,n_2} can be used for detecting balancing selection (DeGiorgio *et al.* 2014).

For the case with two alleles considered above, the expected total branch length is simply $2T_{i,2-i}$. Consider a sample size of three. It can be in one of four possible states, with states 1, 2, 3, and 4 corresponding to situations where 0, 1, 2, and 3 of the sampled alleles are associated with A_1. Going backwards in time, the coalescent process can move between these states via recombination or mutation between allelic classes. For instance, in state 1 all three alleles are associated with A_2, and the process moves to state 2 at rate $3M_{21}$. When there is more than one allele in the same allelic class, coalescence may occur. Again, take state 1 as an example. There are three alleles in allelic class 2, so that the rate of coalescence is $\binom{3}{2}/\hat{p}_2 = 3/\hat{p}_2$. A coalescent event moves the process to one of the three transient states depicted in Figure 1, referred to as states 5, 6, and 7 here. The transition rates between these states, as well as the rates of entering the absorbing state (i.e., the MRCA), are identical to those discussed above (i.e., (2)).

A diagram showing the transition rates between the states in this model can be found in Figure S4. The intensity matrix $\mathbf{\Lambda}$ for this model can be defined in the same way as described above, and is displayed in Supplementary Text S.1. $\mathbf{\Lambda}$ has a block structure:

$$\mathbf{\Lambda} = \begin{bmatrix} \boldsymbol{S}_3 & \boldsymbol{S}_{32} & \underline{\underline{0}} \\ \underline{\underline{0}} & \boldsymbol{S}_2 & \boldsymbol{s}_2 \\ \vec{0} & \vec{0} & 0 \end{bmatrix} \tag{10}$$

where $\underline{\underline{0}}$ is a matrix of zeros. $\boldsymbol{S}_3$ is a 4-by-4 matrix and contains the transition rates between states 1 - 4, all with three alleles. $\boldsymbol{S}_{32}$ is a 4-by-3 matrix and contains the rates of coalescent events that move the process from a state with three alleles to one with only two alleles (i.e., from states 1 - 4 to states 5 - 7). Finally, $\boldsymbol{S}_2$ and $\boldsymbol{s}_2$ are the same as the corresponding elements defined in (3). The sub-intensity matrix $\boldsymbol{S}$ is the 7-by-7 sub-matrix in the upper left corner of $\mathbf{\Lambda}$, and contains the transition rates between all the transient states.

Taking advantage of the block structure, we can calculate the Green's matrix efficiently as:

$$\boldsymbol{U} = -\boldsymbol{S}^{-1} = -\begin{bmatrix} \boldsymbol{S}_3 & \boldsymbol{S}_{32} \\ \underline{\underline{0}} & \boldsymbol{S}_2 \end{bmatrix}^{-1} = \begin{bmatrix} -\boldsymbol{S}_3^{-1} & \boldsymbol{S}_3^{-1}\boldsymbol{S}_{32}\boldsymbol{S}_2^{-1} \\ \underline{\underline{0}} & -\boldsymbol{S}_2^{-1} \end{bmatrix}. \tag{11}$$

Recall that $\boldsymbol{U} = \{u_{ij}\}$ and u_{ij} is the expected amount of time the process spends in (transient) state j prior to reaching the MRCA, provided that the initial state is i. If, for instance, we want to calculate $L_{0,3}$, we first note that the sample is in state 1. The process spends, on average, $\sum_{j=1}^{4} u_{1j}$ in states 1 - 4. Because these states have three alleles, the coalescent genealogy must have three lineages. Thus, these four states contribute $3\sum_{j=1}^{4} u_{1j}$ to $L_{0,3}$. Similarly, states 5 - 7, which contain two alleles, contribute $2\sum_{k=5}^{7} u_{1k}$. Putting these together, we have:

$$L_{0,3} = 3\sum_{j=1}^{4} u_{1j} + 2\sum_{k=5}^{7} u_{1k}. \tag{12}$$

More generally, if the sample is in state i, we can define the initial condition vector as $\boldsymbol{\alpha} = \boldsymbol{e}_i$, where $i \in \{1,2,3,4\}$ and $\boldsymbol{e}_i$ is a 1-by-7 vector whose elements are 0 except that the $i-$th element is 1. If we further define $\boldsymbol{D}^T = (3,3,3,3,2,2,2)$, we have:

$$L_{i,3-i} = \boldsymbol{\alpha}\boldsymbol{U}\boldsymbol{D}. \tag{13}$$

As we will see later, expressing the results this way allows us to accommodate non-equilibrium situations. $\boldsymbol{D}$ is known as the reward vector, and we can use phase-type theory to obtain the distribution and all the moments of the total branch length (Hobolth *et al.* 2019).

The approach can be easily extended to an arbitrary sample size n. As discussed above (see (7)), for data analysis, it is useful to consider the expected total branch length for a random sample of size n, defined as:

$$L = \sum_{i=0}^{n} \binom{n}{i} \hat{p}_1^i \hat{p}_2^{n-i} L_{i,n-i}. \tag{14}$$

In Figure 4, we display L for several combinations of sample sizes and variant frequencies at the selected locus. To make the diversity-elevating effect more visible, we divide L by its neutral expectation (i.e., $2\sum_{i=1}^{n-1} \frac{1}{i}$). It is evident that, as n becomes larger, the sensitivity of L to $\hat{p}_1$ decreases, to the extent that, when $n = 30$, L is effectively independent of $\hat{p}_1$. In addition, the strongest signal of elevated diversity appears when $n = 2$ and $\hat{p}_1 = 0.5$, but becomes less pronounced as n increases. To interpret these observations, recall that, when $n = 2$, $\pi = \theta L$, whereas for larger n, θL is the expected number of segregating sites in the sample, denoted by S. In data analysis, the nucleotide site diversity π is typically estimated from samples containing many alleles, and is known to be most sensitive to intermediate frequency variants (Tajima 1989). On the other hand, S is determined primarily by low frequency variants in the sample. Thus, these results

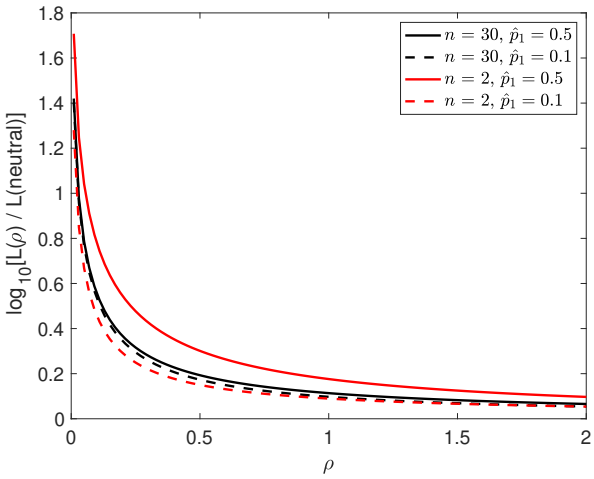

Figure 4 The expected total branch length L for several combinations of sample size (n) and equilibrium frequency of the selected variant A_1 ($\hat{p}_1$). The value of L under balancing selection is divided by its neutral expectation. The y-axis is on the $\log_{10}$ scale.

suggest that S is less informative about balancing selection than π. However, the contrast between S and π can be used as an index of the departure of the SFS from its expectation at neutral equilibrium (Tajima 1989). This clearly points to the importance of considering SFS, which is done in the next subsection.

This way of obtaining the total branch length is an alternative to the recursion method used in previous studies (Hudson and Kaplan 1988; DeGiorgio *et al.* 2014). The advantage of the current approach is that it can be extended to accommodate non-equilibrium dynamics such as population size changes and recent selection (see below). The dimension of the sub-intensity matrix $\boldsymbol{S}$ is now $d = (n+1) + n + ... + 3 = \frac{1}{2}(n-1)(n+4)$. The numerical complexity increases rapidly because numerical matrix inversion requires $O(d^3)$ operations. However, by making use of the block structure (e.g., (11)), the number of operations is reduced to $O((n+1)^3)$. Thus, this approach is computationally feasible for samples of several hundred alleles.

The site frequency spectrum (SFS)

Again, consider a sample of n alleles at the neutral site, with n_1 and n_2 of them associated with A_1 and A_2, respectively. The i-th element of the SFS is defined as the expected number of segregating sites where the derived variant appears i times in the sample ($0 < i < n$). Note that this definition is different from the standard definition for a panmictic population in that it is conditional on n_1 and n_2. Consider the gene tree for the sample. We refer to a lineage (branch) that is ancestral to i alleles in the sample as a lineage of size i ($0 < i < n$). Under the infinite sites model, mutations on a lineage of size i segregate at frequency i in the sample. Let $\phi_i^{(n_1,n_2)}$ be the expected total length of all lineages of size i in the gene tree. The SFS under the infinite sites model can be expressed as $X_i^{(n_1,n_2)} = \theta\phi_i^{(n_1,n_2)}$ (e.g., Polanski and Kimmel 2003). We can calculate $\phi_i^{(n_1,n_2)}$ using phase-type theory with additional book keeping.

To illustrate the calculation, consider a sample of three alleles. Going backwards in time, before the first coalescent event, all the lineages are size one. After the first coalescent event, one lineage is size two, and the other is size one. Thus, the transient states of the coalescent process can be represented by 4-tuples of the form $(a_{1,1}, a_{1,2}, a_{2,1}, a_{2,2})$ where $a_{i,j}$ is the number of lineages of size j that are currently associated with A_i. We have listed all the transient states in Table 1. The first four states contain three lineages, and the last four contain two lineages. We can determine the transition rates between the states using the same arguments that lead to Figures 1 and S4; the intensity matrix $\boldsymbol{\Lambda}$ is displayed in Supplementary Text S.2. Note that $\boldsymbol{\Lambda}$ has the same form as (10), so that we can obtain $\boldsymbol{U}$ using (11).

Table 1 The transient states for a sample size of three

ID	state	ID	state	ID	state	ID	state
1	(0,0,3,0)	2	(1,0,2,0)	3	(2,0,1,0)	4	(3,0,0,0)
5	(0,0,1,1)	6	(1,0,0,1)	7	(0,1,1,0)	8	(1,1,0,0)

As an example, if $n_1 = 2$ and $n_2 = 1$, the starting state is 3, so that only the elements in the third row of $\boldsymbol{U}$ are relevant. Because states 1 - 4 contain three size one lineages, they contribute $3\sum_{i=1}^{4} u_{3i}$ to $\phi_1^{(2,1)}$, but nothing to $\phi_2^{(2,1)}$. The last four states contain one size one lineage and one size two lineage. Thus, they contribute $\sum_{k=5}^{8} u_{3k}$ to both $\phi_1^{(2,1)}$ and $\phi_2^{(2,1)}$. Putting these results together, we have:

$$\begin{cases} \phi_1^{(2,1)} = 3\sum_{i=1}^{4} u_{3i} + \sum_{k=5}^{8} u_{3k} \\ \phi_2^{(2,1)} = \sum_{i=1}^{4} u_{3i} \end{cases} \tag{15}$$

Define the initial condition vector $\boldsymbol{\alpha} = (0,0,1,0,0,0,0,0)$, $\boldsymbol{\phi}^{(2,1)} = (\phi_1^{(2,1)}, \phi_2^{(2,1)})$ and

$$\boldsymbol{D}^T = \begin{bmatrix} 3 & 3 & 3 & 3 & 1 & 1 & 1 & 1 \\ 0 & 0 & 0 & 0 & 1 & 1 & 1 & 1 \end{bmatrix}. \tag{16}$$

We have $\mathbb{E}[\boldsymbol{\phi}^{(2,1)}] = \boldsymbol{\alpha}\boldsymbol{U}\boldsymbol{D}$, which has the same form as (13) and will be useful below when non-equilibrium dynamics are introduced.

We can obtain the other $\boldsymbol{\phi}^{(i,3-i)}$ by defining the appropriate $\boldsymbol{\alpha}$. In addition to the mean, it is also possible to use phase-type theory to obtain the variance of the SFS, as well as the covariance between different elements of the SFS (Hobolth *et al.* 2019). These results are applicable to any sample size $n \geq 2$. We defer showing results regarding the SFS until a later section where a model of recent balancing selection is analysed.

Obtaining the SFS with the phase-type approach has been shown to be numerically more stable and accurate than approaches that rely on solving the diffusion equation numerically (Kern and Hey 2017). However, a limitation is that the size of the state space increases rapidly with n (Andersen *et al.* 2014). This is true even after exploiting the block structure of the sub-intensity matrix $\boldsymbol{S}$. For instance, when $n = 16$, the dimension of the largest sub-matrix in $\boldsymbol{S}$ is 922, but it increases to 3493 when $n = 20$. However, the flexibility of phase-type theory, especially its ability to accommodate complex non-equilibrium models, makes it a useful tool, as we show next.

A model with strong balancing selection and changes in population size

So far we have only considered a model of balancing selection at statistical equilibrium. In this section, we switch our attention to

a non-equilibrium model in which the population size changes in a stepwise manner. Specifically, we consider a diploid, randomly mating population. Looking back in time, its evolutionary history consists of H non-overlapping epochs, such that the effective population size is $N_{e,h}$ in epoch h ($h \in \{1, 2, ..., H\}$). The duration of epoch h is $[t_{h-1}, t_h)$, where $t_0 = 0$ (the present) and $t_H = \infty$. Thus, epoch H, the most ancestral epoch, has an infinite time span, over which the population is at statistical equilibrium. We assume that an autosomal locus is under balancing selection in epoch H, with two alleles A_1 and A_2 at equilibrium frequencies $\hat{p}_1$ and $\hat{p}_2$, respectively. Based on the results shown in the previous sections, we only consider the simplified model without reversible mutation between A_1 and A_2. In addition, we assume that selection is sufficiently strong, and the changes in population size are sufficiently small, that the frequencies of the two alleles remain at $\hat{p}_1$ and $\hat{p}_2$ in the more recent epochs. A similar approach has been applied successfully to modelling the joint effects of background selection and demographic changes (Zeng 2013; Nicolaisen and Desai 2013; Zeng and Corcoran 2015).

As before, consider a neutral site linked to the selected locus, with a sample of n alleles, of which n_1 and n_2 are associated with A_1 and A_2, respectively. Consider the expected total branch length, L_{n_1,n_2}. Here time is scaled in units of $2N_{e,1}$ generations (twice the effective population size in the current epoch). We first note that the current model has the same states as the equilibrium model analysed above (e.g., see Figure S4 for $n = 3$). The main difference between the two models lies in the transition rates between states.

We define the scaled recombination rate as $\rho = 2N_{e,1}r$. The rate at which an allele in allelic class i moves to allelic class j is $M_{ij} = \rho\hat{p}_j$. These have the same form as above (cf. Figure 1). In epoch h, the total number of alleles associated with A_1 in the population is $2N_{e,h}\hat{p}_1$. The probability that two alleles associated with A_1 in the current generation coalesce in the previous generation is $1/(2N_{e,h}\hat{p}_1)$. In other words, the probability that they remain un-coalesced for z generations is:

$$\left(1 - \frac{1}{2N_{e,h}\hat{p}_1}\right)^z \approx \exp\left\{-\frac{z}{2N_{e,h}\hat{p}_1}\right\} = \exp\left\{-\frac{g_h}{\hat{p}_1}t\right\} \quad (17)$$

where $g_h = N_{e,1}/N_{e,h}$ and $t = z/(2N_{e,1})$. Thus, the coalescent rate between a pair of alleles in allelic class 1 is $g_h/\hat{p}_1$ in epoch h. Similarly, the rate for two alleles in allelic class 2 is $g_h/\hat{p}_2$.

In epoch h, the transition rates between the states are constant, and we can define an associated sub-intensity matrix, $\boldsymbol{S}_h$. We have already noted that the states in the current model are the same as those in the equilibrium model. The only difference is that time is now in units of $2N_{e,1}$ generations. Thus, we can obtain $\boldsymbol{S}_h$ by simply replacing ρ and $1/\hat{p}_i$ in the sub-intensity matrix for the equilibrium model (e.g., (10); see also Supplementary Text S.1) by the newly defined equivalents ρ and $g_h/\hat{p}_i$.

Overall, the model has the following parameters: $\hat{p}_1$, ρ, t_1, g_1, t_2, g_2, ..., t_{H-1}, g_{H-1}, and g_H. Among these, $\hat{p}_1$ and ρ are shared across all the epochs, whereas epoch h has two epoch-specific parameters t_h and g_h (note that $t_H = \infty$). We have H sub-intensity matrices: $\boldsymbol{S}_1$, $\boldsymbol{S}_2$, ..., $\boldsymbol{S}_H$. In Supplementary Text S.3, we introduce time-inhomogeneous phase-type theory and prove the following result:

Theorem 1. *Consider a continuous time Markov chain with finite state space $\{1, 2, ..., K, K+1\}$, where states $1, ..., K$ are transient, and state $K+1$ is absorbing. Assume that the time interval $[0, \infty)$ is subdivided into H non-overlapping epochs. The duration of epoch h is $[t_{h-1}, t_h)$, where $1 \le h \le H$, $t_0 = 0$, and $t_H = \infty$. The sub-intensity matrix for epoch h is denoted by $\boldsymbol{S}_h$. Then the Green's matrix is:*

$$\boldsymbol{U} = \sum_{h=1}^{H}\left[\prod_{i=1}^{h-1} e^{\boldsymbol{S}_i d_i}\right]\boldsymbol{U}_h \quad (18)$$

where $d_h = t_h - t_{h-1}$, $\boldsymbol{U}_h = e^{\boldsymbol{S}_h d_h}\boldsymbol{S}_h^{-1} - \boldsymbol{S}_h^{-1}$, and $e^{\boldsymbol{S}_h d_h} = 0$ if $d_h = \infty$.

Applying this theorem requires the evaluation of matrix exponentials. Although this can be done analytically for certain models (e.g., Waltoft and Hobolth 2018), it is not feasible in the models considered here. We instead employ recent numerical methods (Al-Mohy and Higham 2010; Moler and Van Loan 2003), as implemented in the `expm` function in Matlab. The computational cost for obtaining $e^{\boldsymbol{S}_h d_h}$ is typically $O(d^3)$, where d is the dimension of $\boldsymbol{S}_h$. Once $\boldsymbol{U}$ has been calculated using Theorem 1, we can obtain the expected total branch length by $L_{n_1,n_2} = \boldsymbol{\alpha}\boldsymbol{U}\boldsymbol{D}$ (see (13)).

In Figures 5a and b, we show L, the expected total branch length for a random sample of $n = 20$ alleles (see (14)), under either a one-step population size increase or a one-step population size reduction. The population size change occurred at time t before the present. Because L is insensitive to $\hat{p}_1$ when n is relatively large (Figure 4), we only consider $\hat{p}_1 = 0.5$ (the results are qualitatively very similar with $n = 2$; not shown). Neutral diversity levels in genomic regions closely linked to the selected site are affected by recent population size changes to a much smaller extent than regions farther afield. This is because, when ρ is small, the coalescent process is dominated by the slow movement via recombination between the two allelic classes, which dampens the diversity-changing effects of population size changes. In particular, when there has been a recent reduction in population size, this effect protects against the loss of neutral polymorphisms in a larger genomic region (Figure 5b). Consequently, strong balancing selection affects a bigger stretch of the genome and produces a higher peak of diversity in smaller populations, making them easier to detect.

It is also instructive to consider the effects of recent population size changes on LD between the selected and neutral loci. This can be achieved by replacing T and T_A in (9) with $T(t)$ and $T_A(t)$. In Figures 5c and d, we can see that σ^2 converges to its new equilibrium level at a much higher rate than the level of diversity, which is a well-known effect (e.g., McVean 2002). Interestingly, σ^2 appears to approach its new equilibrium in a non-monotonic way. For instance, in Figure 5c, LD levels at $t = 0.4$ are temporarily higher than the equilibrium value (the solid black curve), but become lower than the equilibrium value at $t = 1.3$. In Figure 5d, we can see that the level of LD is higher, and extends further, after the population size reduction. These effects are due to the corresponding reduction in the scaled recombination rate, and explain why balancing selection becomes easier to detect.

A model of recent balanced polymorphism

We now turn our attention to the effects of the recent origin of a balanced polymorphism on patterns of genetic variability. Consider a diploid panmictic population with constant effective population size N_e. At an autosomal locus, a mutation from A_1 (the wild type) to A_2 (the mutant) arises. The fitnesses of the genotypes A_1A_1, A_1A_2, and A_2A_2 are $w_{11} = 1 - s_1$, $w_{12} = 1$, and $w_{22} = 1 - s_2$ ($s_1 > 0$ and $s_2 > 0$; i.e., there is heterozygote

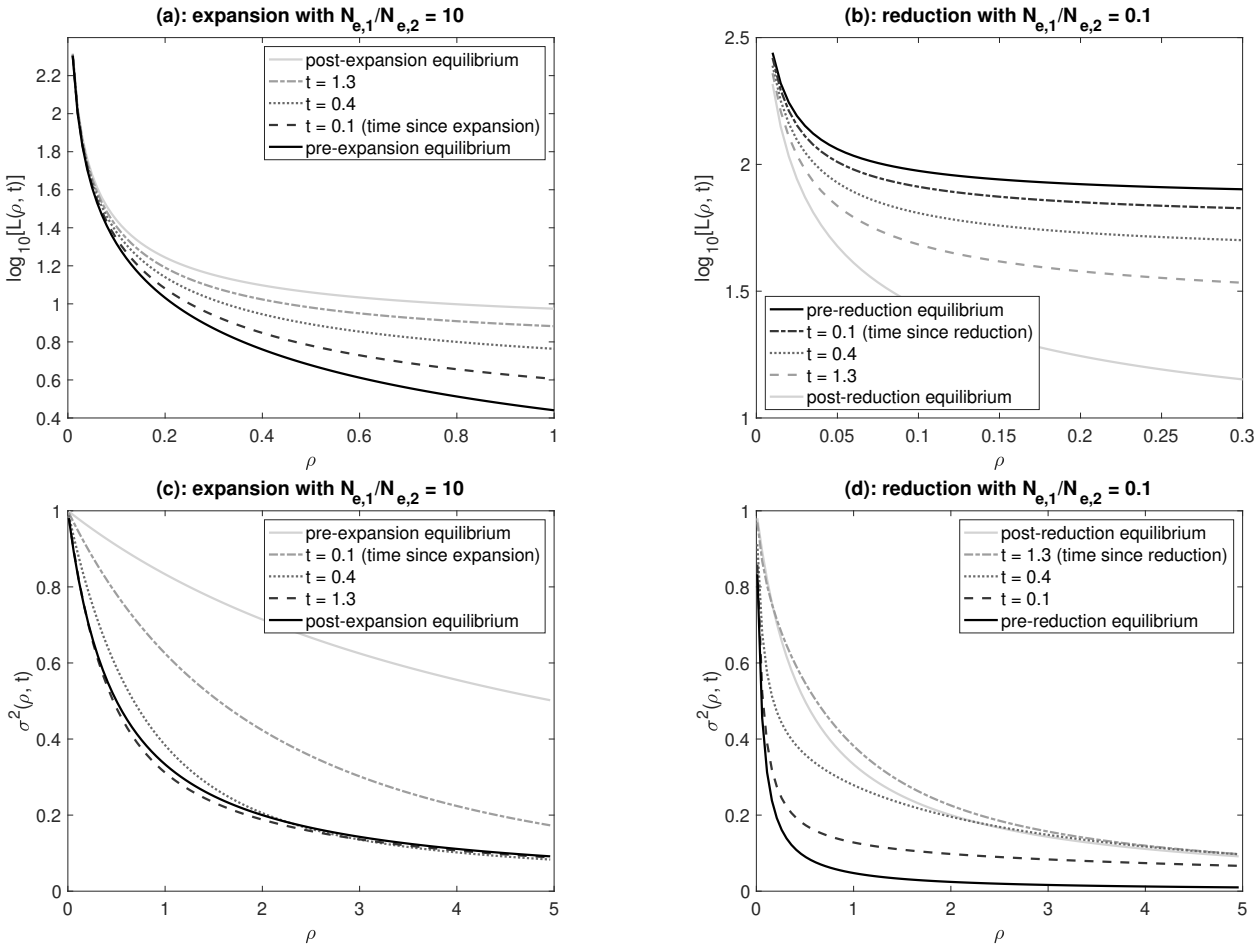

Figure 5 Expected total branch length and LD as a function of ρ and t. The population experienced a one-step change in population size at time t before the present. The population size in the present and ancestral epochs are $N_{e,1}$ and $N_{e,2}$, respectively. Time is scaled in units of $2N_{e,1}$ generations. The selected alleles A_1 and A_2 are at equilibrium frequencies $\hat{p}_1 = \hat{p}_2 = 0.5$. The sample size is $n = 20$.

advantage). As above, we ignore reversible mutation between A_1 and A_2. In what follows, we first use a forward-in-time approach to obtain equations for describing the increase in the frequency of A_2 in the population. We then use the backward-in-time coalescent approach to calculate various measures of sequence variability in linked genomic regions. Wherever appropriate, we present results from a related selective sweep model, so that the two models can be compared.

Frequency of the mutant allele in the population

Let the frequencies of A_1 and A_2 in the current generation be p_1 and p_2, respectively. Let p_2' be the frequency of A_2 in the next generation. Using the standard theory (reviewed in Chap. 2 of Charlesworth and Charlesworth (2010)), the change in allele frequency in one generation due to selection is given by

$$\Delta p_2 = p_2' - p_2 = \frac{p_1 p_2 (w_{2.} - w_{1.})}{\bar{w}} \tag{19}$$

where $w_{1.} = p_1 w_{11} + p_2 w_{12}$, $w_{2.} = p_1 w_{12} + p_2 w_{22}$, and $\bar{w} = p_1 w_{1.} + p_2 w_{2.}$. Assuming that both $s_1 \ll 1$ and $s_2 \ll 1$, $\Delta p_2 \approx p_1 p_2 (w_{2.} - w_{1.}) = p_1 p_2 (p_1 s_1 - p_2 s_2)$. At equilibrium, $\Delta p_2 = 0$, such that the frequencies are $\hat{p}_1 = \frac{s_2}{s_1+s_2}$ and $\hat{p}_2 = \frac{s_1}{s_1+s_2}$.

When $p_2 \ll 1$, $\Delta p_2 \approx s_1 p_2$. This is the same as when A_2 is under positive selection with fitnesses of the three genotypes being $w_{11} = 1$, $w_{12} = 1 + s_1$, and $w_{22} = 1 + 2s_1$, respectively (i.e., there is semi-dominance). Thus, we expect that the initial signals generated by the increase in p_2 to be similar to those from an incomplete selective sweep, referred to here as the "corresponding sweep model".

The similarity between the two selection models means that we can borrow useful results from the selective sweep literature. In particular, after A_2 has been generated by mutation, its frequency must increase rapidly for it to escape stochastic loss when rare. Following an approach first proposed by Maynard Smith (1976), we assume that p_2 increases instantly to $\epsilon = \frac{1}{\gamma_1}$, where $\gamma_1 = 2N_e s_1$ (see also Desai and Fisher 2007). Thereafter, p_2 changes deterministically until its rate of change becomes very slow near the equilibrium point, when the coalescent process (considered in the next sub-section) is effectively the same as at equilibrium. Measuring time in units of $2N_e$ generation, $p_2(t)$ satisfies:

$$\frac{\mathrm{d}p_2}{\mathrm{d}t} = p_1 p_2 (p_1 \gamma_1 - p_2 \gamma_2) \tag{20}$$

where $\gamma_2 = 2N_e s_2$. The solution to this differential equation is

$$\gamma_1 \ln(1 - p_2) + \gamma_2 \ln p_2 - (\gamma_1 + \gamma_2) \ln\left[\gamma_1 - (\gamma_1 + \gamma_2) p_2\right] = \gamma_1 \gamma_2 (t + c) \tag{21}$$

where c is a constant such that $p_2(0) = \epsilon$. We can obtain $p_2(t)$ by fixing t on the right-hand side and solving the equation numerically with respect to p_2.

It is instructive to compare the dynamics of $p_2(t)$ with those for the corresponding sweep model defined above. We assume that the frequency of the positively selected variant A_2 increases instantly to ϵ and grows deterministically until $1-\epsilon$. Let $p_2^*(t)$ be the frequency of A_2 at scaled time t after its frequency has arrived at ϵ. It can be shown that:

$$p_2^*(t) = \frac{\epsilon}{\epsilon + (1-\epsilon)e^{-\gamma_1 t}} \tag{22}$$

(Crow *et al.* 1970; Stephan *et al.* 1992).

A recent study explicitly considered the stochastic phases when the frequency of the positively selected variant A_2 is below ϵ or greater than $1-\epsilon$ (Charlesworth 2020). These two phases contribute relatively little to the fixation time under the current model with strong selection and semi-dominance (see Table 1 of Charlesworth 2020). Furthermore, when the frequency of A_2 is very close to 0 or 1, the coalescent process is effectively the same as under neutrality. Thus, ignoring these two stochastic phases is reasonable for our purposes.

In Figure 6, we display three balancing selection models, all with $\gamma_1 = 500$, but different γ_2 values, so that they have different equilibrium allele frequencies. For comparison, the corresponding sweep model with $\gamma_1 = 500$ is also presented. As can be seen, the allele frequency trajectories for the balancing selection models and the corresponding sweep model are similar only for a rather short period. After that, $p_2(t)$ increases at a much slower pace than $p_2^*(t)$. As shown below, these observations explain the differences between recent balanced polymorphism and the spread of a beneficial mutation with respect to their effects on diversity patterns in nearby genomic regions.

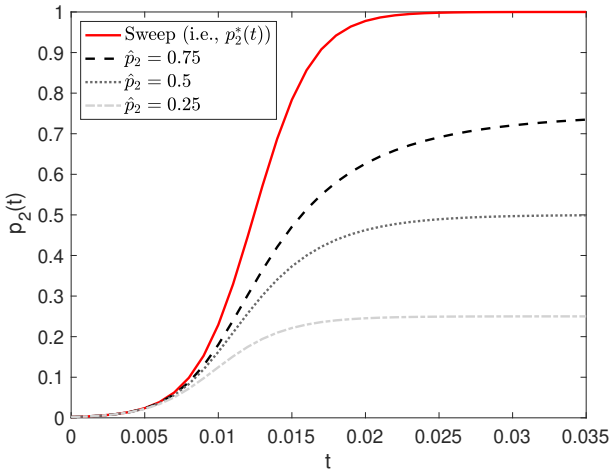

Figure 6 The frequency of the mutant allele A_2 as a function of t (time since its frequency reaches ϵ). $\gamma_1 = 500$. γ_2 is adjusted such that the equilibrium frequency $\hat{p}_2$ is 0.25, 0.5, and 0.75, respectively. The trajectory under the corresponding sweep model is included for comparison.

Total branch length

We extend the coalescent approach developed above for the equilibrium model, in order to calculate the expected total branch length L for a random sample of size n at a linked neutral site (see (14)). The frequency of A_2 at the time of sampling is $p_2(t)$ where t is the time since the frequency of A_2 reaches ϵ, expressed in units of $2N_e$ generations. At time τ before the present ($0 \le \tau < t$), the frequency of A_2 is given by $p_2(t-\tau)$. For $\tau \ge t$, the process reduces to a standard neutral coalescent model with constant population size. To make use of Theorem 1, we divide $[p_2(t), \epsilon)$ into $H-1$ equal-sized bins, such that the h-th bin is $[p_{2,h-1}, p_{2,h})$, where $p_{2,0} = p_2(t)$ and $p_{2,h} = p_2(t) + \frac{h}{H-1}(\epsilon - p_2(t))$ ($h \in \{1, 2, ..., H-1\}$). Let τ_h be the solution to $p_2(t-\tau_h) = p_{2,h}$ given by (21). The corresponding time interval for bin h is $[\tau_{h-1}, \tau_h)$, which is shorter when the frequency of A_2 is changing at a faster rate. Thus, as shown in Figure 7, we have H epochs, with the first $H-1$ in $[0, t)$ and epoch H covering the whole of $[t, \infty)$.

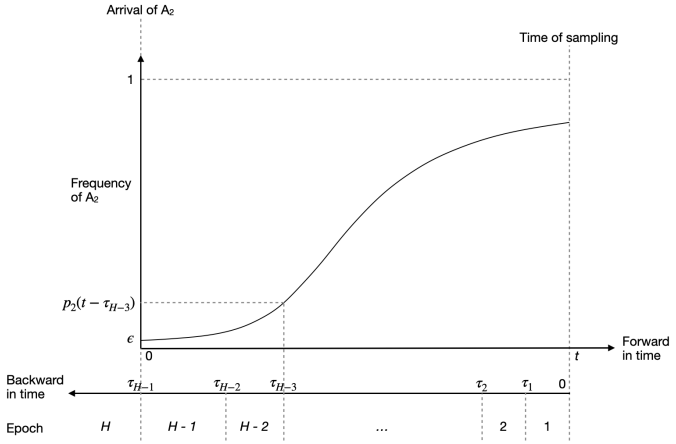

Figure 7 A diagram showing the discretisation scheme used to obtain the expected total branch length and the site frequency spectrum under the model of recent balanced polymorphism.

Consider epoch h with $h < H$. The state space in this epoch is the same as that discussed above for the equilibrium model (see the arguments leading to (10)). Thus, the sub-intensity matrix for this epoch, $\boldsymbol{S}_h$, can be obtained in a similar way (cf., Figure S4). The only complication is that the frequency of A_2 changes within the epoch. However, if the time interval is sufficiently small, we can treat the frequency of A_2 as if it were constant. Here we fix the frequency of A_2 in epoch h to its harmonic mean $q_{2,h}$, which can be calculated as:

$$\frac{1}{q_{2,h}} = \frac{1}{\tau_h - \tau_{h-1}} \int_{\tau_{h-1}}^{\tau_h} \frac{1}{p_2(t-\tau)} \mathrm{d}\tau. \tag{23}$$

We can then obtain $\boldsymbol{S}_h$ by simply replacing $\hat{p}_1$ and $\hat{p}_2$ in the sub-intensity matrix for the equilibrium model with $q_{1,h}$ and $q_{2,h}$, where $q_{1,h} = 1 - q_{2,h}$.

Note that, although the space state is the same for the epochs in $[0, t)$, this is not true for the transition from epoch $H-1$ to epoch H. At the end of epoch $H-1$, if more than one allele is associated with A_2, they coalesce into a single ancestral allele instantly. If the resulting ancestral allele is the only allele left, the process is terminated. Otherwise, if there are also n_1 alleles associated with A_1 at the time, then the n_1+1 alleles enter epoch H and coalesce at rate $\binom{n_1+1}{2}$. Thus, we need a mapping matrix $\boldsymbol{E}_{H-1,H}$, which is defined below (S22) in Supplementary Text S.3, to correct for the differences between the two epochs. For instance, for a sample of two alleles, the state space in $[0, t)$ has three transient states: (0, 2), (1, 1), and (2, 0), where the first and

second number of each tuple represent the number of alleles linked to A_1 and A_2, respectively. However, epoch H has only one transient state, representing two uncoalesced alleles. If the process is in state $(0, 2)$ at the end of $[0, t)$, it terminates with the instant coalescence of the two alleles. If the process is in any of the other two states, it enters epoch H with the same starting condition. Thus $\boldsymbol{E}_{H-1,H}^T = (0, 1, 1)$, where 0 in the first element means it is impossible to enter epoch H via state 1 in epoch $H-1$, and the 1s mean that, if the process is in state 2 or 3 by the end of epoch $H-1$, the process begins epoch H in state 1.

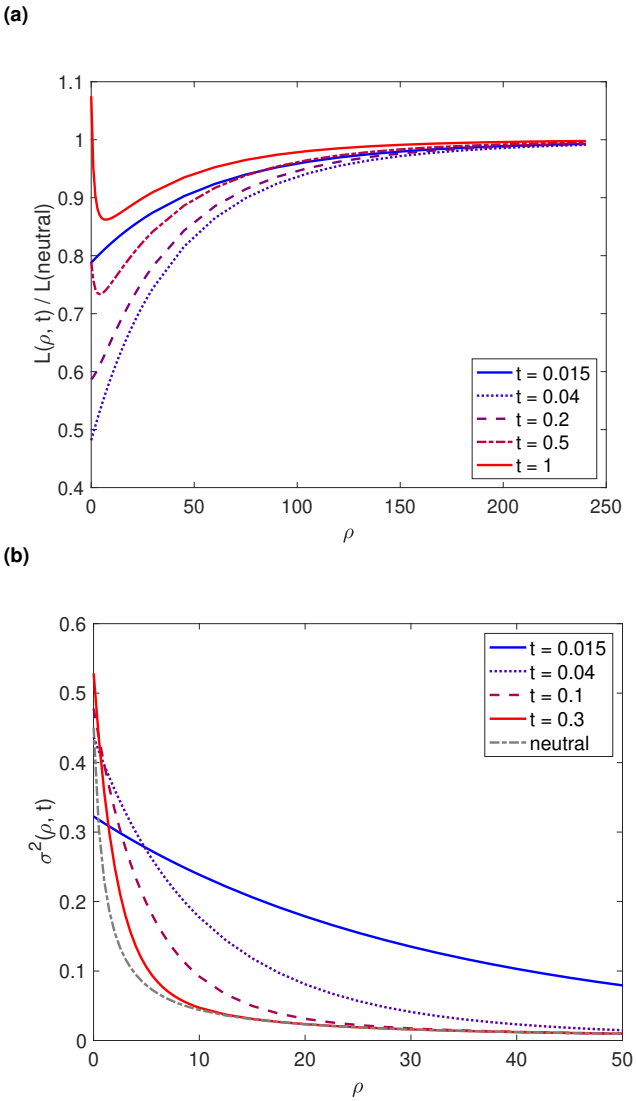

Figure 8 Nucleotide site diversity and LD in genomic regions surrounding a recently-emerged variant under balancing selection. The parameters are $\gamma_1 = 500$ and $\hat{p}_2 = 0.75$ (as in Figure 6). The discretisation scheme has $H = 76$ bins. In (a), the expected total branch length for a sample of $n = 2$ alleles is calculated for various value of t, the time since the frequency of A_2 reaches ϵ. To make the effects more visible, L is divided by its neutral expectation. σ^2 in (b) measures the level of LD between the selected locus and a linked neutral site. For comparison, the neutral expectation of σ^2 is also included.

In all, the model has the following parameters: γ_1, γ_2, t, and ρ. By increasing the number of bins in the discretisation scheme (i.e., H; Figure 7), we can get arbitrarily accurate approximations. The results presented below are based on values of H such that the size of the frequency bins is about 1%. This is a rather conservative choice; using larger bins does not significantly change the results. Once the sub-intensity matrices are defined (i.e., $\boldsymbol{S}_h$ for $1 \le h \le H$), we can obtain $\boldsymbol{U}$ using Theorem 1 (see also Supplementary Text S.3) and $L = \boldsymbol{\alpha U D}$ (see (13)).

Figure 8a shows how neutral diversity levels are affected by a recent balanced polymorphism, using the balancing selection model with $\hat{p}_2 = 0.75$ considered in Figure 6. Initially, the rapid increase in the frequency of A_2 produces a drop in neutral diversity in nearby regions (the solid blue line). The maximum extent of reduction appears when $p_2(t)$ is close to its equilibrium value (the dotted line; $p_2(0.04) = 0.742$). After that, the diversity level starts to recover. Here, the increase in diversity level is fastest for regions closely linked to the selected site, because coalescence is slow when ρ is small. This leads to a U-shaped diversity pattern that persists for some time, which is followed by a rather slow approach to the equilibrium value (Figure S5). These dynamics are qualitatively the same when we consider a larger sample size with 20 alleles, although the reduction in diversity is less pronounced (Figure S6). Similar patterns are also observed for the other two balancing selection models in Figure 6 (Figure S7). The main difference is that models with a smaller $\hat{p}_2$ tend to result in a smaller reduction in neutral diversity. For instance, for the model with $\hat{p}_2 = 0.25$, the maximum reduction in nucleotide site diversity in very tightly linked regions is less than 6% (as opposed to a more than 50% reduction in Figure 8a), making them very difficult to detect from data.

LD between the selected locus and a linked neutral site

It is straightforward to use the method developed in the previous subsection to calculate σ^2. From Figure 8b, we make two observations. First, LD builds up quickly and extends to a large genomic region when the frequency of A_2 is increasing rapidly (blue solid curve vs the neutral curve). This suggests the formation of long haplotypes around the selected locus, which can be used to help detect selection targets, as is done in extended haplotype tests (e.g., Voight *et al.* 2006; Ferrer-Admetlla *et al.* 2014). Second, the level of LD starts to decline before the reduction in diversity is maximal (the dotted curves in Figures 8a and b), suggesting that LD based detection methods will have already lost a substantial amount of their statistical power by this time. This implies that LD and diversity patterns complement each other when it comes to detecting targets of recent balancing selection.

Differences between balancing selection and selective sweeps in their effects on L and LD

We can analyse selective sweep models using the discretisation scheme outlined in Figure 7. In Figure 9a, we compare the balancing selection model shown in Figure 8 to its corresponding sweep model, with respect to their effects on L. Because the frequency of the beneficial allele increases much more rapidly (Figure 6), it causes a more pronounced reduction in diversity than the balanced polymorphism of the same age (before fixation of the beneficial variant). After fixation of the beneficial allele, diversity returns to its neutral level over a time period of the order of $2N_e$ generations, which is much faster than the time it takes for diversity to reach its equilibrium level under balancing selection (Figure S5). The patterns are similar when a larger sample size is considered (Figure S8).

A comparison between the two selection models with respect

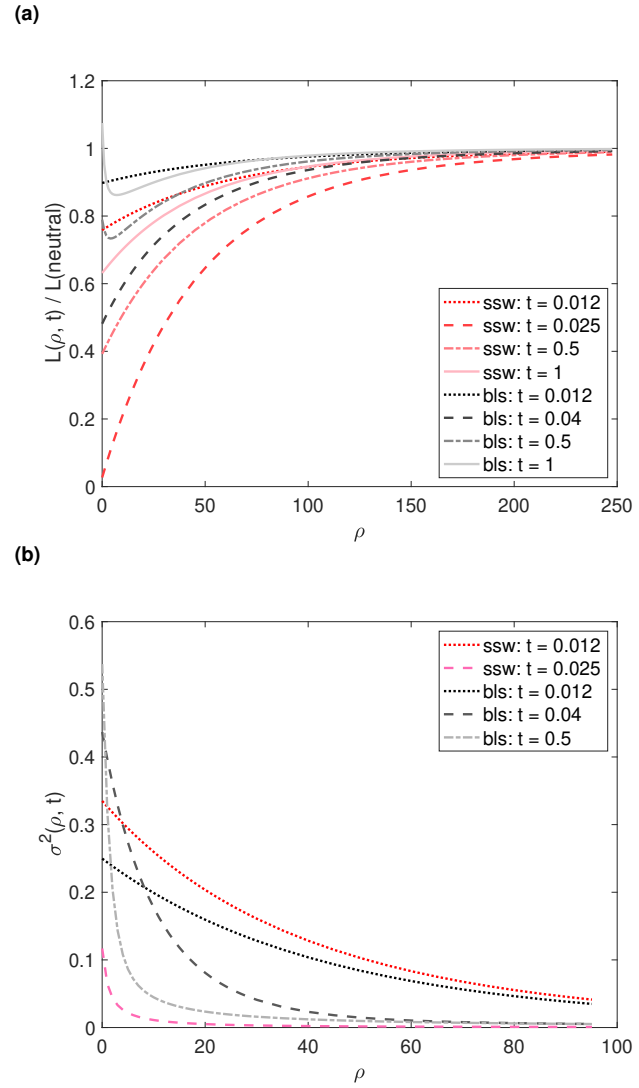

Figure 9 Comparing recent balancing selection with the corresponding sweep model, with respect to their effects on diversity and LD levels in surrounding genomic regions. The parameters of the balancing selection model (bls) are $\gamma_1 = 500$ and $\hat{p}_2 = 0.75$ (i.e., the same as in Figure 8). The corresponding sweep model (ssw) has $\gamma_1 = 500$. In (a), the expected total branch length for a sample of $n = 2$ alleles, divided by its neutral value, is presented. In (b), we consider the level of LD between the selected locus and a linked neutral site, as measured by σ^2. Fixation (taken as the time when the mutant allele frequency reaches $1 - \epsilon$) occurs at $t = 0.025$ under the sweep model. The reduction in diversity reaches its maximum at $t \approx 0.04$ under the balancing selection model.

to their effects on LD patterns in the surrounding neutral region is shown in Figure 9b. Both models result in elevated LD. As expected, the corresponding sweep model leads to a more pronounced build-up of LD (red vs black dotted lines). This suggests that recent balancing selection is harder to detect than a comparable beneficial mutation. Under both models, LD starts to decay before the reduction in diversity is maximal (pink vs grey dashed lines). The decay appears to be much faster under the sweep model. This is because, under the balancing selection model, A_2 approaches an equilibrium frequency, instead of fixation. Therefore, a sizeable genomic region remains at elevated levels of LD with the selected locus for a longer period. Recall that diversity levels also take much longer to reach equilibrium under balancing selection (Figure 9a). Thus, there may well be a bigger window of opportunity for detecting targets of recent balancing selection, despite the fact that the signals they produce tend to be less dramatic than those produced by the corresponding sweep model.

The site frequency spectrum

The SFS can also be obtained using the time discretisation procedure. Here the state space is the same as that detailed for the equilibrium balancing selection model. As above, we obtain the sub-intensity matrix for epoch h by replacing $\hat{p}_1$ and $\hat{p}_2$ in the sub-intensity matrix for the equilibrium model (e.g., Supplementary Text S.2) with $q_{1,h}$ and $q_{2,h}$, respectively. We then use Theorem 1 to calculate $X_i^{(n_1,n_2)}$. It is more instructive to consider the SFS for a sample of n randomly collected alleles, defined as:

$$X_i = \sum_{j=0}^{n} \binom{n}{j} p_1^j p_2^{n-j} X_i^{(j,n-j)} \tag{24}$$

where p_1 and p_2 are the frequencies of A_1 and A_2 at the time of sampling. The effects of selection has on the shape of the SFS are visualised using the ratio $X_i / X_i(\text{neutral})$, where $X_i(\text{neutral}) = 2\theta/i$.

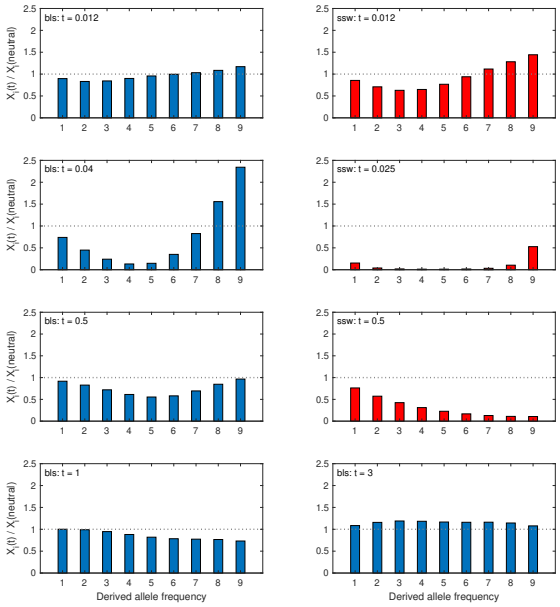

Figure 10 The SFS at various time points after the arrival of the selected variant for a random sample of 10 alleles. The balancing selection (bls) and selective sweep (ssw) models are the same as those shown in Figure 9. The scaled distance between the focal neutral site and the selected site is $\rho = 2$. The reduction in diversity reaches its maximum at $t \approx 0.04$ and 0.025 (fixation) under the balancing selection and selective sweep models, respectively. The SFS under selection is expressed relative to its neutral expectation.

In Figure 10, we present the SFS at different time points since the arrival of the mutant allele, for the balancing selection model and the corresponding sweep model considered in Figures 8 and 9. When the frequency of the selected variant is rapidly increasing in the population, both types of selection produce a U-shaped SFS, with an excess of both low and high frequency derived variants. The extent of distortion is maximised around the time when the reduction in neutral diversity is also the most pronounced (see plots in the second row). The corresponding sweep model has a much bigger effect on the shape of the SFS. For example, under the sweep model, at the time of fixation ($t = 0.025$), $X_9/X_8 = 4.91$ and $X_1/X_2 = 8.05$. In contrast, when the SFS is most distorted under the balancing selection model ($t = 0.04$), $X_9/X_8 = 1.34$ and $X_1/X_2 = 3.29$. The excess of high frequency derived variants quickly disappears after the selected allele has stopped its rapid increase in frequency (plots in the third row), although the SFS remains U-shaped for longer under balancing selection. The plots in the last row shows the transition from a situation with reduced diversity and an excess of low frequency variants to a situation that resembles the pattern expected under long-term balancing selection, with an elevated diversity level and an excess of intermediate frequency variants. Qualitatively similar dynamics have been observed for the balancing selection models with $\hat{p}_2 = 0.5$ and 0.25, respectively, considered in Figure 6. Again, the SFS-distorting effect is weaker when $\hat{p}_2$ is smaller (Figure S9), with the case with $\hat{p}_2 = 0.25$ producing hardly any excess of low and high frequency variants due to the increase in the frequency of A_2.

To investigate the SFS further, we consider π (the nucleotide site diversity) and Watterson's θ_W. Recall that, under the infinite sites model, $\pi = 2\theta T$, where T is defined by (7). Let S be the expected number of segregating sites in a sample of size n. We have $S = \theta L$. Because $\theta_W = S/a_n$ where $a_n = \sum_{i=1}^{n-1} \frac{1}{i}$, we have $\theta_W = \theta L/a_n$. Following Becher *et al.* (2020), we define

$$\Delta\theta_W = 1 - \frac{\pi}{\theta_W} = 1 - \frac{2\theta T}{\theta L/a_n} = 1 - \frac{2a_n T}{L}. \qquad (25)$$

$\Delta\theta_W = 0$ under neutrality, > 0 when there is an excess of rare variants, and < 0 when there is an excess of intermediate frequency variants.

Figure 11 shows $\Delta\theta_W$ for the balancing selection model with $\gamma_1 = 500$ and $\hat{p}_2 = 0.75$ (as in Figures 6 - 10); the corresponding sweep model is also included for comparison. At $t = 0.012$, the balancing selection model produces no obvious deviation from neutrality (black dotted line), whereas the sweep model has already started to cause a significant excess of rare variants (red dotted line). This is consistent with the much slower increase in the frequency of A_2 under balancing selection ($p_2(t) = 0.3$ vs $p_2^*(t) = 0.5$). The extent of deviation caused by the sweep is maximal around the time when A_2 becomes fixed ($t \approx 0.025$; pink dashed line). Under the balancing selection model, the maximum deviation is when the frequency of A_2 becomes close to its equilibrium value ($t \approx 0.04$; grey dashed line), but is less pronounced than under the sweep model. After the maximum is achieved, diversity patterns gradually return to neutrality over $4N_e$ generations under the sweep model. For the balancing selection model, there is a much longer period of non-stationary dynamics as shown by the light blue and blue lines.

It is instructive to compare the three balancing selection models with $\gamma_1 = 500$, but with different equilibrium allele frequencies (Figure 6). The model with $\hat{p}_2 = 0.75$ produces the strongest sweep-like signals, including a reduction in diversity and excess of rare variants (Figure 11 vs Figure S10). At the other extreme, the model with $\hat{p}_2 = 0.25$ effectively emits no such signal (Figure S10). Thus, targets of recent balancing selection with larger $\hat{p}_2$ are easier to detect. However, for older targets of selection, the excess of intermediate frequency variant (i.e., negative $\Delta\theta_W$) is most noticeable for selection targets with $\hat{p}_2 \approx 0.5$ (Figure S10), making them the most amenable to detection. Altogether, it seems that balancing selection targets with low equilibrium allele frequencies (e.g., $\hat{p}_2 \approx 0.25$) are difficult to identify regardless of their age.

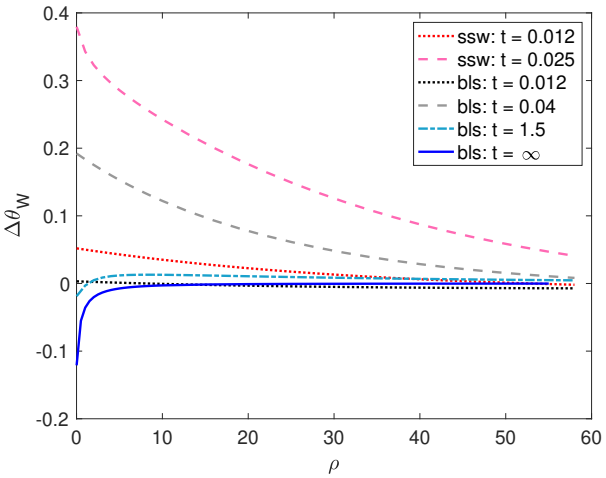

Figure 11 $\Delta\theta_W$ as a function of ρ and t. The two selection models are the same as those considered in Figure 10. "bls: $t = \infty$" corresponds to the equilibrium under balancing selection. The sample size is 10.

Discussion

In this study, we have used the power and flexibility afforded by phase-type theory to study the effects of balancing selection on patterns of genetic variability and LD in nearby genomic regions. Our results go beyond previous attempts in that they provide a unifying framework for calculating important statistics for both equilibrium and nonequilibrium cases. In what follows, we discuss how our results can be used in data analyses and future method developments. We will also discuss the usefulness of phase-type theory in general.

Accommodating other biological factors

Here we have only considered selection on an autosomal locus in a randomly mating population. However, our results can be readily extended to accommodate other important biological factors. Take self-fertilization as an example. Let s be the selfing rate and $F = s/(2-s)$ be the corresponding inbreeding coefficient. For this model, $N_e = N/(1+F)$, where N is the number of breeding individuals (Charlesworth 2009). Because selfing increases the frequency of homozygotes in the population, it reduces the effective frequency of recombination to $r_e = (1-F)r$, where r is the autosomal recombination rate in a random-mating population (Nordborg 1997; see Hartfield and Bataillon 2020 for a more accurate expression for r_e). Finally, for the model of recent balancing selection, we also need to consider the effects of selfing on the frequency trajectory of A_2. This can be achieved

by replacing (20) with:

$$\frac{\mathrm{d}p_2}{\mathrm{d}t} = p_1 p_2 \left[(1-F)(p_1\gamma_1 - p_2\gamma_2) + F(\gamma_1 - \gamma_2)\right]. \qquad (26)$$

Other factors, including division into two sexes, mode of inheritance (e.g., X-linkage vs autosomal), and background selection, can also be modelled (Charlesworth 2009; Vicoso and Charlesworth 2009; Glémin 2012; Charlesworth 2020; Hartfield and Bataillon 2020).

Detecting long-term balancing selection

We have examined two models of long-term balancing selection, one with a constant population size and the other with recent demographic changes. We confirm the well-known result that long-term balancing selection leads to elevated diversity and LD in a relatively small region in the immediate vicinity of the locus under selection (Charlesworth 2006; Fijarczyk and Babik 2015). We also find that, under our two-allele model, the strength of these signals is highest when the equilibrium frequencies of the selected variants are close to 50%, and weakens when the frequencies become unequal (Figures 2 and 3), so that genome scan methods are biased towards detecting selection targets where the selected variants are more common (Bitarello *et al.* 2018; Siewert and Voight 2020).

Our results can be used to improve existing methods for detecting balancing selection. For example, the T_1 test by DeGiorgio *et al.* (2014), which has been shown to be among the most powerful, is based on L, the expected total branch length. The recursion equations DeGiorgio *et al.* (2014) used to obtain L assumes a constant population size. We can now relax this assumption by incorporating changes in population size. The increase in the strength of signals of long-term balancing selection after population size reduction (Figure 5b) points to the importance of incorporating non-equilibrium demographic dynamics, which may help to increase statistical power and reduce false positive rates. On the other hand, the results presented in Figure 4 shows that the number of segregating sites in the sample, denoted by S, does not capture all of the information about balancing selection in the data. Instead, statistical power can be gained by making use of the SFS. Recall that $S = \theta L$. This explains why the T_1 test (based on L) is often less powerful than the T_2 test (based on the SFS) (DeGiorgio *et al.* 2014). However, DeGiorgio *et al.* (2014) obtained the SFS via stochastic simulations, due to a lack of analytical methods. Here we have filled this gap. As above, it is of interest to extend the T_2 test, so that it includes both the equilibrium and non-equilibrium models.

Detecting recent balancing selection

It has long been suggested that signals generated by recent balancing selection should be similar to those generated by incomplete sweeps (Charlesworth 2006; Fijarczyk and Babik 2015). Empowered by time-inhomogeneous phase-type theory, we present a systematic comparison between these two models. The dynamics of a recent balanced polymorphism are similar to those of a beneficial mutation of comparable strength when the frequency of the mutant allele is no more than a few percent in the population (Figure 6). This period is only a small fraction of the time it takes for the beneficial mutation to become fixed. In addition, the sigmoid shape of the allele frequency trajectories clearly indicates that the rate of allele frequency change in this period is slower than when the mutant allele is more common. Combining these two factors, it is unsurprising that, when the allele frequency trajectories under the two models start to diverge, neither model produce a noticeable effect on diversity patterns in nearby genomic regions (data not shown). Thus, this initial period of identity contributes very little signal.

After the initial period, the frequency of the beneficial mutation increases rapidly. In contrast, the rate of growth under the balancing selection model is much slower, especially when the equilibrium frequency of the mutant allele is low (Figure 6). Nonetheless, the increase in frequency of a recent balanced polymorphism does produce sweep-like diversity patterns, but they are more subtle than for sweeps. These include reductions in genetic variability, a skew towards high and low frequency derived variants in the SFS, and a build-up of LD between the selected and linked neutral sites (Figures 8 - 11). In addition, similar to sweeps, the maximum build-up of LD appears before the reduction in diversity levels and the distortion of the SFS are most pronounced, suggesting that these signals complement each other. Thus, we expect that these patterns, which exist in a period around the time at which the frequency of the mutant gets close to its equilibrium value, should be detectable by methods designed for identifying sweeps (Booker *et al.* 2017; Pavlidis and Alachiotis 2017), as has been shown previously (Zeng *et al.* 2006). An open question is whether it is possible to distinguish between these two types of selection. Another question is related to the result that recent balancing selection causes diversity and LD patterns to be in a non-equilibrium state for a long period. It is unclear whether these patterns can be exploited for detecting selection targets.

It is informative to compare the three balancing selection models with equilibrium allele frequencies $\hat{p}_2 = 0.25$, 0.5, and 0.75, respectively (Figure 6). The model with $\hat{p}_2 = 0.75$ produces the strongest sweep-like patterns (e.g., Figure 10 vs Figure S9). These recent selection targets should be easiest to detect, although they may also be the most difficult to be separated from sweeps. On the other hand, although selection targets with $\hat{p}_2 = 0.5$ are not as easy to detect when they are young, they produce the strongest deviation from neutrality if they have been maintained for a sufficiently long period of time (Figures 2, 3, and S10), suggesting that they are most likely to be picked up by methods for detecting long-term selection targets. Finally, it seems that selection targets with $\hat{p}_2 = 0.25$ are the most difficult to detect regardless of the age of the mutant allele.

Using phase-type theory to assess the accuracy of simpler approximations

We have shown the ease for which phase-type theory can be used to analyse complex models. In some cases, this can lead to simple analytic solutions (e.g., (5) and (6)). When explicit analytic solutions are difficult to obtain, phase-type theory can serve as a useful tool to search for simpler approximations. Take the model of recent balancing selection as an example. By using a large number of bins in the discretisation scheme (Figure 7), we can obtain results that are effectively exact. It is, however, impossible to write them as simple equations. Nonetheless, if we make an additional assumption that the recombination frequency between the selected locus and the neutral locus is not too high relative to the strength of selection, we can adopt the methods developed in Charlesworth (*under review*) for selective sweeps, such that they can be used to obtain the expected pairwise coalescence time (see Supplementary Text S.5 for details).

We can assess the reliability of this approximation by comparing its results with those obtained using the phase-type method. As expected, the approximate results match the exact results

closely when the recombination rate is low (e.g., $\rho = 1$ in Figure 12). For higher recombination rates, the approximation underestimates the diversity-reducing effect of the spread of A_2. The main reason for this discrepancy is because the approximation assumes that the recombination rate is low, and the "sweep phase" is short. When these assumptions hold, once recombination during the sweep phase has moved a lineage from allelic class 2 to allelic class 1, back migration to allelic class 2 can be ignored. Although these assumptions work well for selective sweep models Charlesworth (*under review*), they are less suitable for the model of recent balancing selection, because the increase in allele frequency is much slower, leading to a longer sweep phase, and hence more opportunities for recombination. Thus, by preventing lineages from being moved back into allelic class 2, the approximation artificially slows down the rate of coalescence during the sweep phase, explaining the overestimation of pairwise coalescence time. Using results produced by phase-type theory as the baseline is desirable because, unlike stochastic simulations, these results are analytical, making comparisons straightforward and small differences easier to detect.

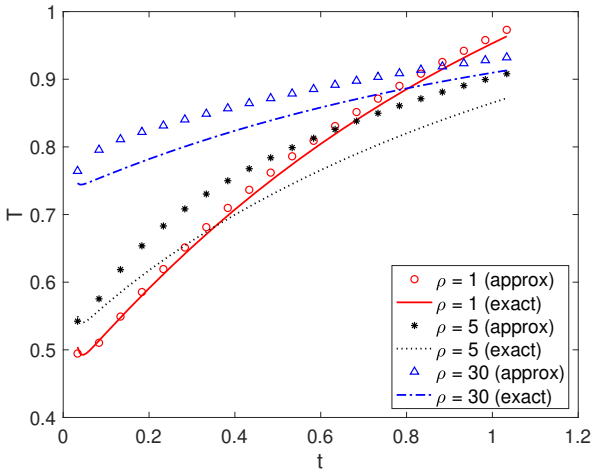

Figure 12 Comparing expected pairwise coalescence times obtained by phase-type theory (exact) and an approximation assuming low recombination rates. The model of recent balancing selection model has the following parameters: $\gamma_1 = 500$ and $\hat{p}_2 = 0.75$ (i.e., the same as in Figures 8 - 11). t is the time since the arrival of A_2. The discretisation scheme has $H = 76$ epochs. Details of the approximation are given in Supplementary Text S.5.

Applying phase-type theory to other population genetic models

Phase-type theory is highly flexible and can be applied to many different models in population genetics. For example, Hobolth *et al.* (2019) used a time-homogeneous version of the model to study the standard Kingman's coalescent with and without recombination, coalescent models with multiple mergers, and coalescent models with seed banks. They show the ease for which useful results can be obtained (e.g., all the moments of the pairwise coalescence time, the covariance in coalescence times between two linked loci, or the SFS). By extending the framework to non-equilibrium cases, we make this approach applicable to a yet larger class of models. In addition to Theorem 1 (see also Corollary 1), we have also proved Theorem 2 in Supplementary Text S.4, which can be used to obtain the second moment of the mean coalescence time. We can now, for instance, introduce population size fluctuations into the models considered by Hobolth *et al.* (2019). Even for models that have been analysed before using other approaches (e.g., Matuszewski *et al.* 2017), it is worth exploring whether the new theory provides a better alternative, both in terms of ease of analysis and numerical stability of the resulting method, which may be beneficial for parameter estimation purposes (e.g., Kern and Hey 2017).

The phase-type approach may be particularly useful for models that involve selection on a single locus at which the frequencies of the selected variants are "tightly regulated" in the sense that the dynamics of the allele frequencies over time are deterministic (Maynard Smith and Haigh 1974; Kaplan *et al.* 1988; Coop and Ralph 2012). These include the balancing selection models considered here, selective sweep models (Barton 1998; Kim and Stephan 2002; Kim and Nielsen 2004; Ewing *et al.* 2010; Charlesworth 2020; Hartfield and Bataillon 2020), soft sweeps caused by recurrent mutation or migration (Pennings and Hermisson 2006), incomplete sweeps (Vy and Kim 2015), and recurrent sweeps (Kaplan *et al.* 1989; Kim 2006; Campos and Charlesworth 2019).

Here, we have briefly considered selective sweep models with semi-dominance and compared it to the corresponding balancing selection model (see (22) and Figures 6, 9 - 11). In a related study, we will use the phase-type approach to look at some of the sweep models listed above more systematically (K. Zeng and B. Charlesworth, *in prep*). As discussed above, because we can use phase-type theory to obtain exact solutions, it provides a convenient way to determine the accuracy of existing approximations. For instance, for the sweep model with semi-dominance, a widely-used approximation assumes that there is no coalescence during the sweep phase, such that the the gene tree for a set of alleles sampled immediately after a sweep has a simple "star shape" (Maynard Smith and Haigh 1974; Barton 2000; Durrett and Schweinsberg 2004). However, a recent study of the pairwise coalescence time suggests that this approximation can be rather inaccurate when the ratio of the recombination rate to the selection coefficient is high Charlesworth (*under review*). It is important to also assess the effect of this simplifying assumption on the SFS, given that both nucleotide site diversity and the SFS are informative when it comes to estimating the strength and prevalence of (recurrent) sweeps (Corbett-Detig *et al.* 2015; Elyashiv *et al.* 2016; Booker *et al.* 2017; Comeron 2017). In addition, we can also explore the joint effects of recurrent sweeps and recent population size changes. These are not well understood, and are important for estimating the relative importance of background selection and recurrent sweeps in shaping genome-wide patterns of variability (e.g., Johri *et al.* 2020).

Literature Cited

Al-Mohy, A. H. and N. J. Higham, 2010 A new scaling and squaring algorithm for the matrix exponential. SIAM Journal on Matrix Analysis and Applications **31**: 970–989.

Andersen, L. N., T. Mailund, and A. Hobolth, 2014 Efficient computation in the im model. J Math Biol **68**: 1423–51.

Andres, A. M., M. J. Hubisz, A. Indap, D. G. Torgerson, J. D. Degenhardt, *et al.*, 2009 Targets of balancing selection in the human genome. Molecular Biology and Evolution **26**: 2755–2764.

Bakker, E. G., C. Toomajian, M. Kreitman, and J. Bergelson, 2006 A genome-wide survey of r gene polymorphisms in arabidopsis. The Plant Cell **18**: 1803–1818.

Barton, N. H., 1998 The effect of hitch-hiking on neutral genealogies. Genetics Research **72**: 123–133.

Barton, N. H., 2000 Genetic hitchhiking. Philosophical Transactions of the Royal Society of London. Series B: Biological Sciences **355**: 1553–1562.

Becher, H., B. C. Jackson, and B. Charlesworth, 2020 Patterns of genetic variability in genomic regions with low rates of recombination. Current Biology **30**: 94–100 e3.

Bitarello, B. D., C. de Filippo, J. C. Teixeira, J. M. Schmidt, P. Kleinert, *et al.*, 2018 Signatures of long-term balancing selection in human genomes. Genome Biology and Evolution **10**: 939–955.

Booker, T. R., B. C. Jackson, and P. D. Keightley, 2017 Detecting positive selection in the genome. BMC biology **15**: 98.

Campos, J. L. and B. Charlesworth, 2019 The effects on neutral variability of recurrent selective sweeps and background selection. Genetics **212**: 287–303.

Castric, V. and X. Vekemans, 2004 Plant self-incompatibility in natural populations: a critical assessment of recent theoretical and empirical advances. Molecular Ecology **13**: 2873–2889.

Charlesworth, B., 2009 Effective population size and patterns of molecular evolution and variation. Nature Reviews Genetics **10**: 195–205.

Charlesworth, B., 2020 How long does it take to fix a favorable mutation, and why should we care? The American Naturalist **195**: 753–771.

Charlesworth, B., 2020 How good are predictions of the effects of selective sweeps on levels of neutral diversity? *Under review*.

Charlesworth, B. and D. Charlesworth, 2010 *Elements of Evolutionary Genetics*. Roberts and Company Publishers, Greenwood Village (Colorado).

Charlesworth, B., M. Nordborg, and D. Charlesworth, 1997 The effects of local selection, balanced polymorphism and background selection on equilibrium patterns of genetic diversity in subdivided populations. Genetical Research **70**: 155–174.

Charlesworth, D., 2006 Balancing selection and its effects on sequences in nearby genome regions. PLoS Genetics **2**: 379–384.

Cheng, X. H. and M. DeGiorgio, 2019 Detection of shared balancing selection in the absence of trans-species polymorphism. Molecular Biology and Evolution **36**: 177–199.

Comeron, J. M., 2017 Background selection as null hypothesis in population genomics: insights and challenges from drosophila studies. Philosophical Transactions of the Royal Society B: Biological Sciences **372**: 20160471.

Connallon, T. and A. G. Clark, 2014 Balancing selection in species with separate sexes: Insights from fisher's geometric model. Genetics **197**: 991–1006.

Coop, G. and P. Ralph, 2012 Patterns of neutral diversity under general models of selective sweeps. Genetics **192**: 205–224.

Corbett-Detig, R. B. and D. L. Hartl, 2012 Population genomics of inversion polymorphisms in drosophila melanogaster. PLoS Genet **8**: e1003056.

Corbett-Detig, R. B., D. L. Hartl, and T. B. Sackton, 2015 Natural selection constrains neutral diversity across a wide range of species. PLoS Biol **13**: e1002112.

Crow, J. F., M. Kimura, *et al.*, 1970 *An introduction to population genetics theory.*. New York, Evanston and London: Harper & Row, Publishers.

DeGiorgio, M., K. E. Lohmueller, and R. Nielsen, 2014 A model-based approach for identifying signatures of ancient balancing selection in genetic data. PLoS Genetics **10**: e1004561.

Desai, M. M. and D. S. Fisher, 2007 Beneficial mutation selection balance and the effect of linkage on positive selection. Genetics **176**: 1759–98.

Dobzhansky, T., 1970 *Genetics of the evolutionary process*. Columbia University Press, New York, fourth edition.

Durrett, R. and J. Schweinsberg, 2004 Approximating selective sweeps. Theoretical population biology **66**: 129–138.

Eanes, W. F., 1999 Analysis of selection on enzyme polymorphisms. Annual Review of Ecology and Systematics **30**: 301–326.

Elyashiv, E., S. Sattath, T. T. Hu, A. Strutsovsky, G. McVicker, *et al.*, 2016 A genomic map of the effects of linked selection in drosophila. PLoS genetics **12**: e1006130.

Ewing, G., J. Hermisson, P. Pfaffelhuber, and J. Rudolf, 2010 Selective sweeps for recessive alleles and for other modes of dominance. Journal of Mathematical Biology **63**: 399–431.

Ferrer-Admetlla, A., M. Liang, T. Korneliussen, and R. Nielsen, 2014 On detecting incomplete soft or hard selective sweeps using haplotype structure. Molecular biology and evolution **31**: 1275–1291.

Fijarczyk, A. and W. Babik, 2015 Detecting balancing selection in genomes: limits and prospects. Molecular Ecology **24**: 3529–3545.

Fisher, R. A., 1922 On the dominance ratio. Proceedings of the Royal Society of Edinburgh **42**: 321–341.

Gilbert, K. J., F. Pouyet, L. Excoffier, and S. Peischl, 2020 Transition from background selection to associative overdominance promotes diversity in regions of low recombination. Current Biology **30**: 101–107 e3.

Glémin, S., 2012 Extinction and fixation times with dominance and inbreeding. Theoretical Population Biology **81**: 310–316.

Hartfield, M. and T. Bataillon, 2020 Selective sweeps under dominance and inbreeding. G3 **10**: 1063–1075.

Hedrick, P. W., 2011 Population genetics of malaria resistance in humans. Heredity **107**: 283–304.

Hobolth, A., A. Siri-Jegousse, and M. Bladt, 2019 Phase-type distributions in population genetics. Theoretical Population Biology **127**: 16–32.

Hudson, R. R. and N. L. Kaplan, 1988 The coalescent process in models with selection and recombination. Genetics **120**: 831–840.

Innan, H. and M. Nordborg, 2003 The extent of linkage disequilibrium and haplotype sharing around a polymorphic site. Genetics **165**: 437–444.

Johnston, S. E., J. Gratten, C. Berenos, J. G. Pilkington, T. H. Clutton-Brock, *et al.*, 2013 Life history trade-offs at a single locus maintain sexually selected genetic variation. Nature **502**: 93–95.

Johri, P., B. Charlesworth, and J. D. Jensen, 2020 Toward an evolutionarily appropriate null model: Jointly inferring demography and purifying selection. Genetics **215**: 173–192.

Kaplan, N. L., T. Darden, and R. R. Hudson, 1988 The coalescent process in models with selection. Genetics **120**: 819–829.

Kaplan, N. L., R. R. Hudson, and C. H. Langley, 1989 The" hitchhiking effect" revisited. Genetics **123**: 887–899.

Kern, A. D. and J. Hey, 2017 Exact calculation of the joint allele frequency spectrum for isolation with migration models. Genetics **207**: 241–253.

Kim, K. W., B. C. Jackson, H. Zhang, D. P. L. Toews, S. A. Taylor,

et al., 2019 Genetics and evidence for balancing selection of a sex-linked colour polymorphism in a songbird. Nat Commun **10**: 1852.

Kim, Y., 2006 Allele frequency distribution under recurrent selective sweeps. Genetics **172**: 1967–1978.

Kim, Y. and R. Nielsen, 2004 Linkage disequilibrium as a signature of selective sweeps. Genetics **167**: 1513–1524.

Kim, Y. and W. Stephan, 2002 Detecting a local signature of genetic hitchhiking along a recombining chromosome. Genetics **160**: 765–777.

Kimura, M., 1969 The number of heterozygous nucleotide sites maintained in a finite population due to steady flux of mutations. Genetics **61**: 893–903.

Kupper, C., M. Stocks, J. E. Risse, N. Dos Remedios, L. L. Farrell, *et al.*, 2016 A supergene determines highly divergent male reproductive morphs in the ruff. Nature Genetics **48**: 79–83.

Kwiatkowski, D. P., 2005 How malaria has affected the human genome and what human genetics can teach us about malaria. The American Journal of Human Genetics **77**: 171–192.

Leffler, E. M., Z. Gao, S. Pfeifer, L. Segurel, A. Auton, *et al.*, 2013 Multiple instances of ancient balancing selection shared between humans and chimpanzees. Science **339**: 1578–1582.

Matuszewski, S., M. E. Hildebrandt, G. Achaz, and J. D. Jensen, 2017 Coalescent processes with skewed offspring distributions and nonequilibrium demography. Genetics **208**: 323–338.

Maynard Smith, J., 1976 What determines the rate of evolution? American Naturalist **110**: 331–338.

Maynard Smith, J. and J. Haigh, 1974 The hitch-hiking effect of a favourable gene. Genetics Research **23**: 23–35.

McVean, G. A., 2002 A genealogical interpretation of linkage disequilibrium. Genetics **162**: 987–991.

Moler, C. and C. Van Loan, 2003 Nineteen dubious ways to compute the exponential of a matrix, twenty-five years later. SIAM review **45**: 3–49.

Nagylaki, T., 1980 The strong-migration limit in geographically structured populations. Journal of mathematical biology **9**: 101–114.

Nicolaisen, L. E. and M. M. Desai, 2013 Distortions in genealogies due to purifying selection and recombination. Genetics **195**: 221–230.

Nordborg, M., 1997 Structured coalescent processes on different time scales. Genetics **146**: 1501–1514.

Ohta, T. and M. Kimura, 1971 Linkage disequilibrium between two segregating nucleotide sites under the steady flux of mutations in a finite population. Genetics **68**: 571.

Pavlidis, P. and N. Alachiotis, 2017 A survey of methods and tools to detect recent and strong positive selection. Journal of Biological Research-Thessaloniki **24**.

Pennings, P. S. and J. Hermisson, 2006 Soft sweeps ii—molecular population genetics of adaptation from recurrent mutation or migration. Molecular Biology and Evolution **23**: 1076–1084.

Polanski, A. and M. Kimmel, 2003 New explicit expressions for relative frequencies of single-nucleotide polymorphisms with application to statistical inference on population growth. Genetics **165**: 427–436.

Sellis, D., B. J. Callahan, D. A. Petrov, and P. W. Messer, 2011 Heterozygote advantage as a natural consequence of adaptation in diploids. Proceedings of the National Academy of Sciences of the United States of America **108**: 20666–20671.

Siewert, K. M. and B. F. Voight, 2020 Betascan2: Standardized statistics to detect balancing selection utilizing substitution data. Genome Biology and Evolution p. in the press.

Slatkin, M., 1991 Inbreeding coefficients and coalescence times. Genetical Research **58**: 167–175.

Spurgin, L. G. and D. S. Richardson, 2010 How pathogens drive genetic diversity: Mhc, mechanisms and misunderstandings. Proceedings of the Royal Society B: Biological Sciences **277**: 979–988.

Stephan, W., T. H. E. Wiehe, and M. W. Lenz, 1992 The effect of strongly selected substitutions on neutral polymorphism - analytical results based on diffusion-theory. Theoretical Population Biology **41**: 237–254.

Strobeck, C., 1983 Expected linkage disequilibrium for a neutral locus linked to a chromosomal arrangement. Genetics **103**: 545–555.

Tajima, F., 1989 Statistical method for testing the neutral mutation hypothesis by dna polymorphism. Genetics **123**: 585–595.

Takahata, N., 1990 A simple genealogical structure of strongly balanced allelic lines and trans-species evolution of polymorphism. Proceedings of the National Academy of Sciences of the United States of America **87**: 2419–2423.

Takahata, N. and M. Nei, 1990 Allelic genealogy under overdominant and frequency-dependent selection and polymorphism of major histocompatibility complex loci. Genetics **124**: 967–978.

Takahata, N. and Y. Satta, 1998 Footprints of intragenic recombination at hla loci. Immunogenetics **47**: 430–441.

van Diepen, L. T., Å. Olson, K. Ihrmark, J. Stenlid, and T. Y. James, 2013 Extensive trans-specific polymorphism at the mating type locus of the root decay fungus heterobasidion. Molecular Biology and Evolution **30**: 2286–2301.

Vekemans, X. and M. Slatkin, 1994 Gene and allelic genealogies at a gametophytic self-incompatibility locus. Genetics **137**: 1157–65.

Vicoso, B. and B. Charlesworth, 2009 Effective population size and the faster-x effect: An extended model. Evolution **63**: 2413–2426.

Voight, B. F., S. Kudaravalli, X. Wen, and J. K. Pritchard, 2006 A map of recent positive selection in the human genome. PLoS biology **4**.

Vy, H. M. T. and Y. Kim, 2015 A composite-likelihood method for detecting incomplete selective sweep from population genomic data. Genetics **200**: 633–649.

Waltoft, B. L. and A. Hobolth, 2018 Non-parametric estimation of population size changes from the site frequency spectrum. Statistical Applications in Genetics and Molecular Biology **17**.

Watterson, G., 1975 On the number of segregating sites in genetical models without recombination. Theoretical Population Biology **7**: 256–276.

Zeng, K., 2013 A coalescent model of background selection with recombination, demography and variation in selection coefficients. Heredity **110**: 363–371.

Zeng, K. and P. Corcoran, 2015 The effects of background and interference selection on patterns of genetic variation in subdivided populations. Genetics **201**: 1539–54.

Zeng, K., Y.-X. Fu, S. Shi, and C.-I. Wu, 2006 Statistical tests for detecting positive selection by utilizing high-frequency variants. Genetics **174**: 1431–1439.

Supplementary text

S.1 The intensity matrix for calculating the total branch length of a sample size of three

$\boldsymbol{S}_2$ and $\boldsymbol{s}_2$ in (10) are the same as the corresponding elements defined in (3).

$$\boldsymbol{S}_3 = \begin{pmatrix} -3M_{21} - \frac{3}{\hat{p}_2} & 3M_{21} & 0 & 0 \\ M_{12} & -M_{12} - 2M_{21} - \frac{1}{\hat{p}_2} & 2M_{21} & 0 \\ 0 & 2M_{12} & -2M_{12} - M_{21} - \frac{1}{\hat{p}_1} & M_{21} \\ 0 & 0 & 3M_{12} & -3M_{12} - \frac{3}{\hat{p}_1} \end{pmatrix} \tag{S1}$$

and

$$\boldsymbol{S}_{32} = \begin{pmatrix} \frac{3}{\hat{p}_2} & 0 & 0 \\ 0 & \frac{1}{\hat{p}_2} & 0 \\ 0 & \frac{1}{\hat{p}_1} & 0 \\ 0 & 0 & \frac{3}{\hat{p}_1} \end{pmatrix}. \tag{S2}$$

S.2 The intensity matrix for calculating the SFS for a sample size of three

The sub-matrices in (10) for the model leading to Table 1 are given below.

$$\boldsymbol{S}_3 = \begin{pmatrix} -3M_{21} - \frac{3}{\hat{p}_2} & 3M_{21} & 0 & 0 \\ M_{12} & -M_{12} - 2M_{21} - \frac{1}{\hat{p}_2} & 2M_{21} & 0 \\ 0 & 2M_{12} & -2M_{12} - M_{21} - \frac{1}{\hat{p}_1} & M_{21} \\ 0 & 0 & 3M_{12} & -3M_{12} - \frac{3}{\hat{p}_1} \end{pmatrix}. \tag{S3}$$

$$\boldsymbol{S}_{32} = \begin{pmatrix} \frac{3}{\hat{p}_2} & 0 & 0 & 0 \\ 0 & \frac{1}{\hat{p}_2} & 0 & 0 \\ 0 & 0 & \frac{1}{\hat{p}_1} & 0 \\ 0 & 0 & 0 & \frac{3}{\hat{p}_1} \end{pmatrix}. \tag{S4}$$

$$\boldsymbol{S}_2 = \begin{pmatrix} -2M_{21} - \frac{1}{\hat{p}_2} & M_{21} & M_{21} & 0 \\ M_{12} & -M_{12} - M_{21} & 0 & M_{21} \\ M_{12} & 0 & -M_{12} - M_{21} & M_{21} \\ 0 & M_{12} & M_{12} & -2M_{12} - \frac{1}{\hat{p}_1} \end{pmatrix}. \tag{S5}$$

$$\boldsymbol{s}_2^T = \begin{pmatrix} \frac{1}{\hat{p}_2} & 0 & 0 & \frac{1}{\hat{p}_1} \end{pmatrix}. \tag{S6}$$

S.3 A non-equilibrium phase-type model

Consider a continuous time Markov chain with finite state space $\{1, 2, ..., K, K+1\}$, where states $1, ..., K$ are transient, and state $K+1$ is absorbing. It is assumed that the time interval $[0, \infty)$ is subdivided into H non-overlapping epochs. The duration of epoch h is $[t_{h-1}, t_h)$, where $1 \leq h \leq H$, $t_0 = 0$, and $t_H = \infty$. The intensity matrix for epoch h is constant and takes the form:

$$\boldsymbol{\Lambda}_h = \begin{pmatrix} \boldsymbol{S}_h & \boldsymbol{s}_h \\ \vec{0} & 0 \end{pmatrix} \tag{S7}$$

where $\boldsymbol{S}_h$ the K-by-K sub-intensity matrix, and $\boldsymbol{s}_h$ is the K-by-1 exit rate vector.

Define

$$\begin{cases} d_h = t_h - t_{h-1} \\ \mathbb{h}(t) = \min\{h : 1 \leq h \leq H \text{ and } t_{h-1} \leq t < t_h\} \\ d_{\mathbb{h}(t)} = t - t_{\mathbb{h}(t)-1} \end{cases} \tag{S8}$$

The transition probability between time 0 and time t is given by:

$$\boldsymbol{P}(t) = \left[\prod_{h=1}^{\mathbb{h}(t)-1} \boldsymbol{P}_h(d_h) \right] \boldsymbol{P}_{\mathbb{h}(t)}(d_{\mathbb{h}(t)}) \tag{S9}$$

where $\boldsymbol{P}_h(t)$ is the transition matrix for epoch h. From standard Markov chain theory, we know that:

$$\boldsymbol{P}_h(t) = \begin{pmatrix} e^{\boldsymbol{S}_h t} & \vec{1} - e^{\boldsymbol{S}_h t}\vec{1} \\ \vec{0} & 1 \end{pmatrix}. \tag{S10}$$

Define

$$\boldsymbol{S}(t) = \left[\prod_{h=1}^{\mathbb{h}-1} e^{\boldsymbol{S}_h d_h} \right] e^{\boldsymbol{S}_{\mathbb{h}} d_{\mathbb{h}}}. \tag{S11}$$

We can rewrite (S9) in a more compact form:

$$\boldsymbol{P}(t) = \begin{pmatrix} \boldsymbol{S}(t) & \vec{1} - \boldsymbol{S}(t)\vec{1} \\ \vec{0} & 1 \end{pmatrix}. \tag{S12}$$

The probability that the process jumps to the absorbing state in the time interval $[t, t+\mathrm{d}t)$ is given by:

$$f(t)\mathrm{d}t = \sum_{i=1}^{K} \alpha_i \sum_{j=1}^{K} s_{ij}(t) s_j(t) \mathrm{d}t = \boldsymbol{\alpha}\boldsymbol{S}(t)\boldsymbol{s}(t)\mathrm{d}t \tag{S13}$$

where $s_{ij}(t)$ are elements of $\boldsymbol{S}(t)$, and $s_j(t)$ are elements of $\boldsymbol{s}_{\mathbb{h}(t)}$, the exit rate vector at time t. The Laplace transform of $f(t)$ is defined as:

$$\mathcal{L}(z) = \int_0^{\infty} e^{-zt} \boldsymbol{\alpha}\boldsymbol{S}(t)\boldsymbol{s}(t)\mathrm{d}t \tag{S14}$$

Noting that $\boldsymbol{s}_h = -\boldsymbol{S}_h\vec{1}$ and substituting (S11) into (S14) leads to:

$$\mathcal{L}(z) = -\boldsymbol{\alpha}\sum_{h=1}^{H}\left[\prod_{i=1}^{h-1}e^{\boldsymbol{S}_i d_i}\right]\left[\int_{t_{h-1}}^{t_h} e^{-(z\boldsymbol{I}-\boldsymbol{S}_h)t}\mathrm{d}t\right]e^{-\boldsymbol{S}_h t_{h-1}}\boldsymbol{S}_h\vec{1}, \tag{S15}$$

where $\boldsymbol{I}$ is the identity matrix. To evaluate the integral, we define $\boldsymbol{A}_h(z) = \boldsymbol{A}_h = -(z\boldsymbol{I} - \boldsymbol{S}_h)$. Because all eigenvalues of $\boldsymbol{A}_h$ have strictly negative real parts (Hobolth *et al.*, 2019), $\lim_{t\to\infty} e^{\boldsymbol{A}_h t} = 0$. We obtain:

$$\int_{t_{h-1}}^{t_h} e^{\boldsymbol{A}_h t}\mathrm{d}t = \boldsymbol{A}_h^{-1}\left(e^{\boldsymbol{A}_h t_h} - e^{\boldsymbol{A}_h t_{h-1}}\right). \tag{S16}$$

Taking the derivative with respect to z, we obtain:

$$\frac{\mathrm{d}}{\mathrm{d}z}\int_{t_{h-1}}^{t_h} e^{\boldsymbol{A}_h t}\mathrm{d}t = \boldsymbol{A}_h^{-1}\left[(\boldsymbol{A}_h^{-1} - t_h\boldsymbol{I})e^{\boldsymbol{A}_h t_h} - (\boldsymbol{A}_h^{-1} - t_{h-1}\boldsymbol{I})e^{\boldsymbol{A}_h t_{h-1}}\right]. \tag{S17}$$

Noting that the mean time to absorption is given by $-\frac{\mathrm{d}\mathcal{L}(z)}{\mathrm{d}z}\big|_{z=0}$ and that $\boldsymbol{A}_h(0) = \boldsymbol{S}_h$, we have:

$$\mathbb{E}[\mathcal{T}] = \boldsymbol{\alpha}\sum_{h=1}^{H}\left[\prod_{i=1}^{h-1}e^{\boldsymbol{S}_i d_i}\right]\left[(\boldsymbol{S}_h^{-1} - t_h\boldsymbol{I})e^{\boldsymbol{S}_h d_h} + t_{h-1}\boldsymbol{I} - \boldsymbol{S}_h^{-1}\right]\vec{1}. \tag{S18}$$

Rearranging the equation, we arrive at Theorem 1. To facilitate further discussion, we state this Theorem in a slightly different way:

Corollary 1. *Let $\boldsymbol{\alpha} = (\alpha_1, ..., \alpha_K)$, where α_i is the probability that the initial state is i and $\sum_{i=1}^{K}\alpha_i = 1$. Let $\mathcal{T}$ be a random variable representing the time to absorption. We have:*

$$\mathbb{E}[\mathcal{T}] = \boldsymbol{\alpha}\boldsymbol{U}\vec{1} \tag{S19}$$

where

$$\begin{cases}\boldsymbol{U} = \sum_{h=1}^{H}\left[\prod_{i=1}^{h-1}e^{\boldsymbol{S}_i d_i}\right]\boldsymbol{U}_h \\ \boldsymbol{U}_h = e^{\boldsymbol{S}_h d_h}\boldsymbol{S}_h^{-1} - \boldsymbol{S}_h^{-1}\end{cases} \tag{S20}$$

and $e^{\boldsymbol{S}_h d_h} = 0$ if $d_h = \infty$.

We have also derived an expression for the second moment of $\mathcal{T}$ in Theorem 2 in Supplementary Text S.4.

Let $u_{ij,h}$ represent the elements of $\boldsymbol{U}_h$. $u_{ij,h}$ is the amount of time the process spends in state j during $[t_{h-1}, t_h)$ given that it is in state i at time t_{h-1}. That is, $\boldsymbol{U}_h$ is the Green's matrix for the h-th epoch. Also note that element i in the vector $\boldsymbol{\alpha}\prod_{j=1}^{h-1}e^{\boldsymbol{S}_j d_j}$ gives the probability that the process is in state i at time t_{h-1}. Thus, Corollary 1 shows that, under this stepwise model, the Green's matrix for the entire process $\boldsymbol{U}$ is the weighted average of the Green's matrices of all the constituent epochs.

As noted in the main text, the expectation of both L_{n_1,n_2} and $\boldsymbol{\phi}^{(n_1,n_2)}$ can be written in the form $\boldsymbol{\alpha}\boldsymbol{U}\boldsymbol{D}$. Let Y represent either of these two random variables. Corollary 1 tells us that:

$$\mathbb{E}[Y] = \sum_{h=1}^{H}\mathbb{E}[Y_h] \tag{S21}$$

where

$$\mathbb{E}[Y_h] = \boldsymbol{\alpha}\left[\prod_{i=1}^{h-1} e^{\boldsymbol{S}_i d_i}\right]\boldsymbol{U}_h\boldsymbol{D} \tag{S22}$$

which is the expected contribution from epoch h.

We have so far assumed that the state space is the same across epochs. This restriction can be relaxed. Let the size of the state space in epoch h be K_h. Let $\boldsymbol{E}_{h-1,h}$ be a K_{h-1}-by-K_h matrix that defines the mapping of the states from epoch $h-1$ to epoch h ($h = 1, ..., H$ and $E_{01} = \boldsymbol{I}$, the identity matrix). Corollary 1 holds if we replace $\prod_{i=1}^{h-1} e^{\boldsymbol{S}_i d_i}$ by $(\prod_{i=1}^{h-1} \boldsymbol{E}_{i-1,i} e^{\boldsymbol{S}_i d_i})\boldsymbol{E}_{h-1,h}$. For (S21), we additionally need to replace $\boldsymbol{D}$ by an epoch-specific $\boldsymbol{D}_h$.

S.4 The second moment of the mean time to absorption

The second moment of $\mathcal{T}$ is given by $\frac{\mathrm{d}^2\mathcal{L}(z)}{\mathrm{d}z^2}\big|_{z=0}$. The second derivative with respect to z for the integral in (S16) reads:

$$\frac{\mathrm{d}^2}{\mathrm{d}z^2}\int_{t_{h-1}}^{t_h} e^{\boldsymbol{A}_h t}\mathrm{d}t = \boldsymbol{A}_h^{-1}\sum_{k=0}^{1}(-1)^k e^{\boldsymbol{A}_h t_{h-k}}\left[\boldsymbol{A}_h^{-2} + \left(\boldsymbol{A}_h^{-1} - t_{h-k}\boldsymbol{I}\right)^2\right] \tag{S23}$$

Substituting (S23) into (S15) leads to the following result.

Theorem 2. *The second moment of the mean time to absorption, $\mathbb{E}[\mathcal{T}^2]$, is given by:*

$$\boldsymbol{\alpha}\sum_{h=1}^{H}\left[\prod_{i=1}^{h-1} e^{\boldsymbol{S}_i d_i}\right]\sum_{k=0}^{1}(-1)^{k+1} e^{\boldsymbol{S}_h(t_{h-k}-t_{h-1})}\left[\boldsymbol{S}_h^{-2} + \left(\boldsymbol{S}_h^{-1} - t_{h-k}\boldsymbol{I}\right)^2\right]\vec{1}. \tag{S24}$$

S.5 Approximating the expected pairwise coalescence time under the model of recent balancing selection

As in the main text, we assume that a new allele A_2 has arisen by mutation, and has spread to a frequency $\tilde{p}_2$ that is close to its equilibrium value under balancing selection, which is $\hat{p}_2 = s_1/(s_1+s_2)$ with heterozygote advantage. Providing that the recombination rate is not too high relative to the strength of selection, the expected coalescence time for a pair of A_2 alleles sampled at frequency $\tilde{p}_2$ can be obtained from Equations 9, 10, 11a and A1-A3 of Charlesworth (*under review*), where $\Delta\pi$ in his Equation 11a is equivalent to the reduction in the mean pairwise coalescence time relative to the neutral value of $2N_e$ generations. To obtain $\Delta\pi$, $\tilde{p}_2$ replaces q_2 in Equations 9, 10 and A1-A3 of Charlesworth (*under review*), where the selection parameters in Equations A1-A3 are $\gamma = 2N_e s_1$, $a = 1$, and $b = -(s_1+s_2)/s_1$. At the time when $\tilde{p}_2$ is reached, the values of the expected coalescent times (on the timescale of $2N_e$ generations) for a pair of A_1 alleles is approximately equal to 1.

In addition, the possibility that a recombination event introduces the neutral site from an A_1 allele onto an A_2 background, thereby reducing the initial divergence at the neutral site between an A_1 and A_2 pair, is modelled by using Equation A3a of Charlesworth (*under review*) with q_2 replaced with $1-p_2$ and q with $1-\epsilon$, to yield a probability of an

A_1 to A_2 recombination event of P_{r1}. In addition, the selection parameters a and b should be replaced with $a + b$, and $-b$, respectively. It is assumed that such a recombination event is followed by coalescence with a non-recombined neutral site associated with A_2, with a coalescence time equal to the duration of sweep, t_s, as given by 21 with $p_2 = \tilde{p}_2$. The divergence between an A_1 and A_2 pair at the time of sampling is then given by $1-P_{r1}(1-t_s)$.

A simple way to obtain the pairwise coalescence times at an arbitrary time after the allele frequency $\tilde{p}_2$ has been reached is to consider the recursion relations for the corresponding pairwise expected diversity measures with a neutral mutation rate of u under the infinite sites mutation model and assuming that the frequency of A_2 remains close to its equilibrium value. The scaled mutation rate in the absence of selection, $\theta = 2N_e u$, is sufficiently small that second-order terms in θ can be neglected (Malécot, 1969, p. 40; Wiehe and Stephan, 1993, Equation 6a). Writing π_{ij} for the expected diversity for a pair of alleles A_i and A_j, and using primes for their values in a new generation, and neglecting second-order terms, we have:

$$\pi'_{11} = \left[1 - \left(2u + 2r\hat{p}_2 + \frac{1}{2N_e\hat{p}_1}\right)\right]\pi_{11} + r\hat{p}_1\pi_{12} + 2u \tag{S25a}$$

$$\pi'_{12} = 2r\hat{p}_2\pi_{11} + [1 - (2u + r)]\,\pi_{12} + 2r\hat{p}_1\pi_{22} + 2u \tag{S25b}$$

$$\pi'_{22} = r\hat{p}_2\pi_{12} + \left[1 - \left(2u + 2r\hat{p}_1 + \frac{1}{2N_e\hat{p}_2}\right)\right]\pi_{22} + 2u \tag{S25c}$$

The coefficients of the π_{ij} in these equations provide the corresponding coefficients for the recursions of the deviations of the π_{ij} from their equilibrium values, thereby eliminating the term in $2u$ on the right-hand sides of the equations. If the π_{ij} are scaled relative to their expected value 2θ in the absence of selection, and u is set arbitrarily close to zero, solving for equilibrium gives π_{ij} values relative to 2θ that are equivalent to the equilibrium coalescent times given by (6), as can be verified by direct calculation.

By setting u to zero in (S25), and using the scaled the π_{ij}, we thus obtain a recursion for the deviations from equilibrium of the corresponding expected pairwise coalescence times on the timescale of $2N_e$ generations. While it is possible in principle to diagonalize the relevant matrix, and express the solution for an arbitrary time after reaching $\tilde{p}_2$ in term of its eigenvalues and eigenvectors, in practice it is simpler to iterate the matrix with assigned numerical values of the parameters. In order to save computation time, a relatively small value of N_e can be used, and the recombination parameters rescaled accordingly to represent a much larger N_e with the same value of $\rho = 2N_e r$. The initial relative values of π_{11}, π_{12}, and π_{22} are 1, 1, and $1 - \Delta\pi$.

References

Charlesworth, B., 2020 How good are predictions of the effects of selective sweeps on levels of neutral diversity? *Under review.*

Hobolth, A., A. Siri-Jegousse, and M. Bladt, 2019 Phase-type distributions in population genetics. Theoretical Population Biology **127**: 16–32.

Malécot, G., 1969 *The mathematics of heredity*. Freeman.

Wiehe, T. H. and W. Stephan, 1993 Analysis of a genetic hitchhiking model, and its application to dna polymorphism data from drosophila melanogaster. Mol Biol Evol **10**: 842–854.

Supplementary figures

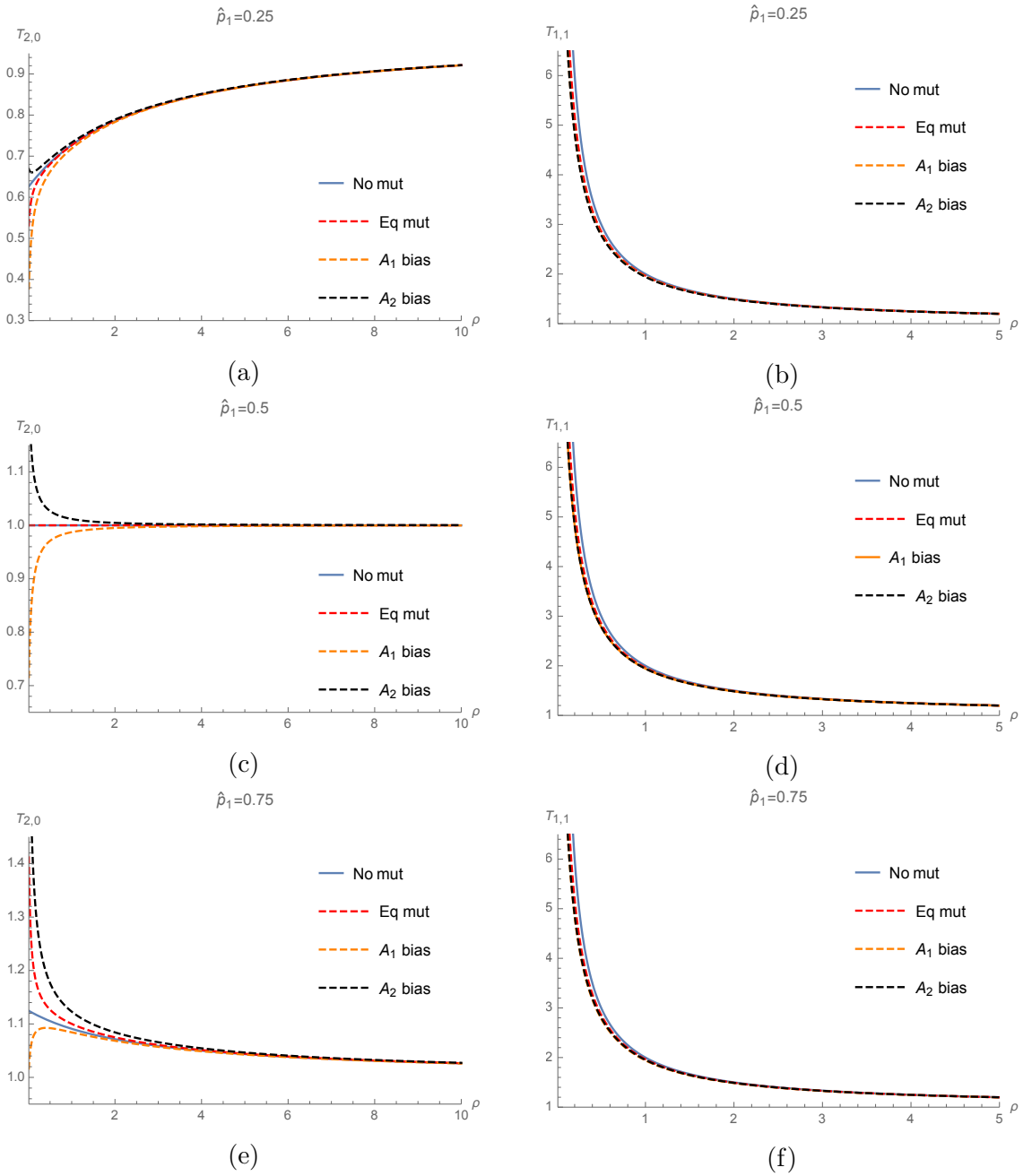

Figure S1: Expected coalescence time for a pair of alleles as a function of ρ. The selected alleles A_1 and A_2 are at equilibrium frequencies $\hat{p}_1$ and $1-\hat{p}_1$. "No mut" means $\mu_{ij}=0$ (i.e., (6)). "Eq mut" means $\mu_{ij}=0.02$. "A_1 bias" means $\mu_{12}=0.01$ and $\mu_{21}=0.05$. "A_2 bias" means $\mu_{12}=0.05$ and $\mu_{21}=0.01$. The scales of the axes are different.

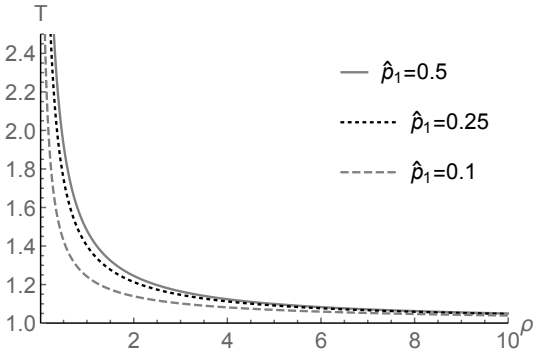

(a) Equal mutation rate

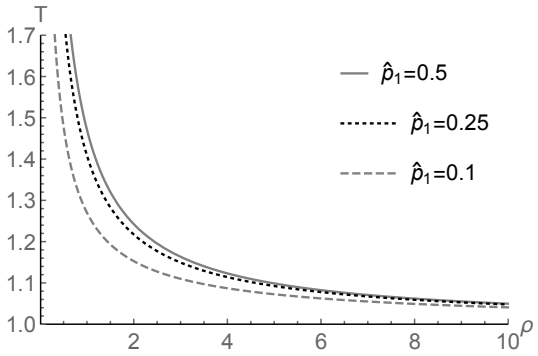

(b) A_1 bias

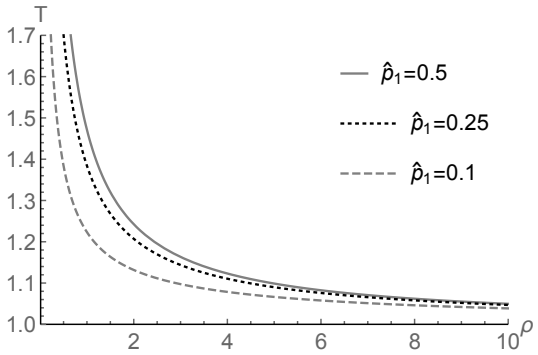

(c) A_2 bias

Figure S2: Expected coalescence time for a pair of alleles as a function of ρ. The selected alleles A_1 and A_2 are at equilibrium frequencies $\hat{p}_1$ and $1 - \hat{p}_1$. "Equal mutation rate" means $\mu_{ij} = 0.02$. "A_1 bias" means $\mu_{12} = 0.01$ and $\mu_{21} = 0.05$. "A_2 bias" means $\mu_{12} = 0.05$ and $\mu_{21} = 0.01$.

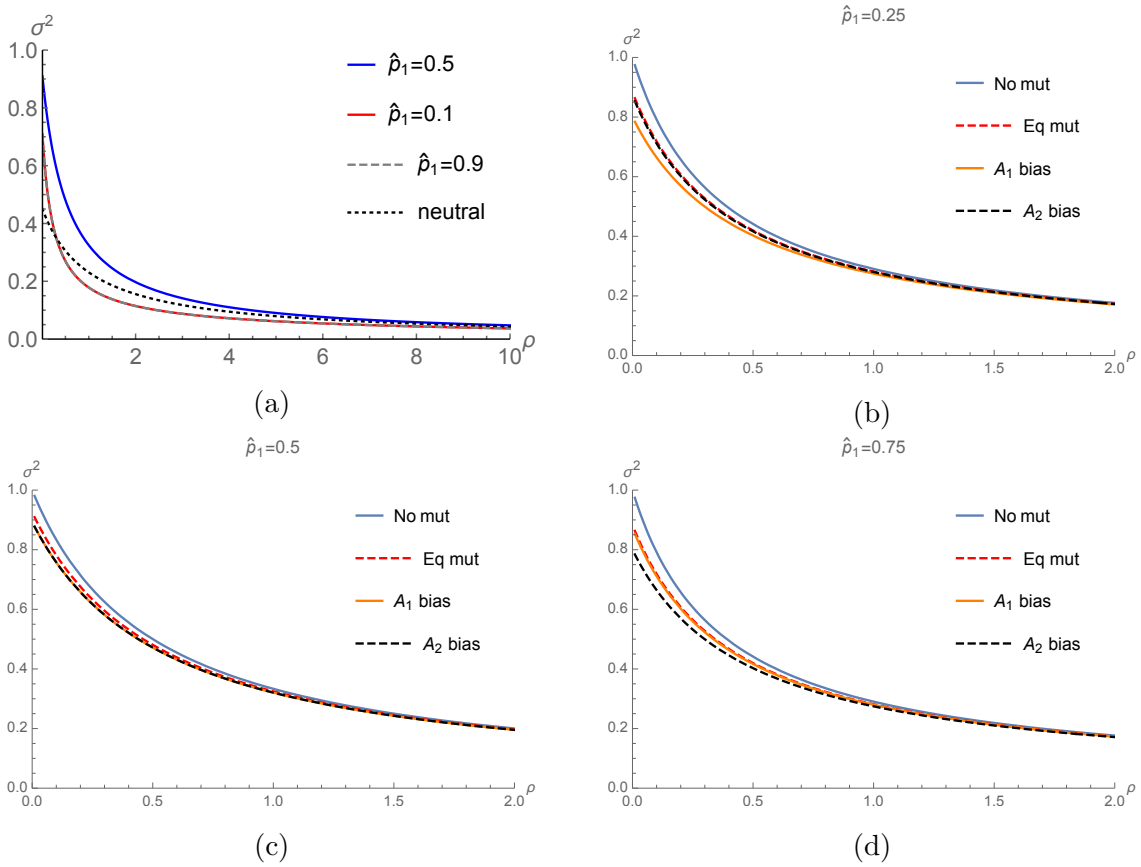

Figure S3: The level of LD between the selected and neutral loci as a function of ρ. In (a), the mutation rates between A_1 and A_2 are $\mu_{12} = \mu_{21} = 0.02$. In (b) - (d), for a given $\hat{p}_1$, different mutation rates are considered. "No mut" means $\mu_{ij} = 0$. "Eq mut" means $\mu_{ij} = 0.02$. "A_1 bias" means $\mu_{12} = 0.01$ and $\mu_{21} = 0.05$. "A_2 bias" means $\mu_{12} = 0.05$ and $\mu_{21} = 0.01$.

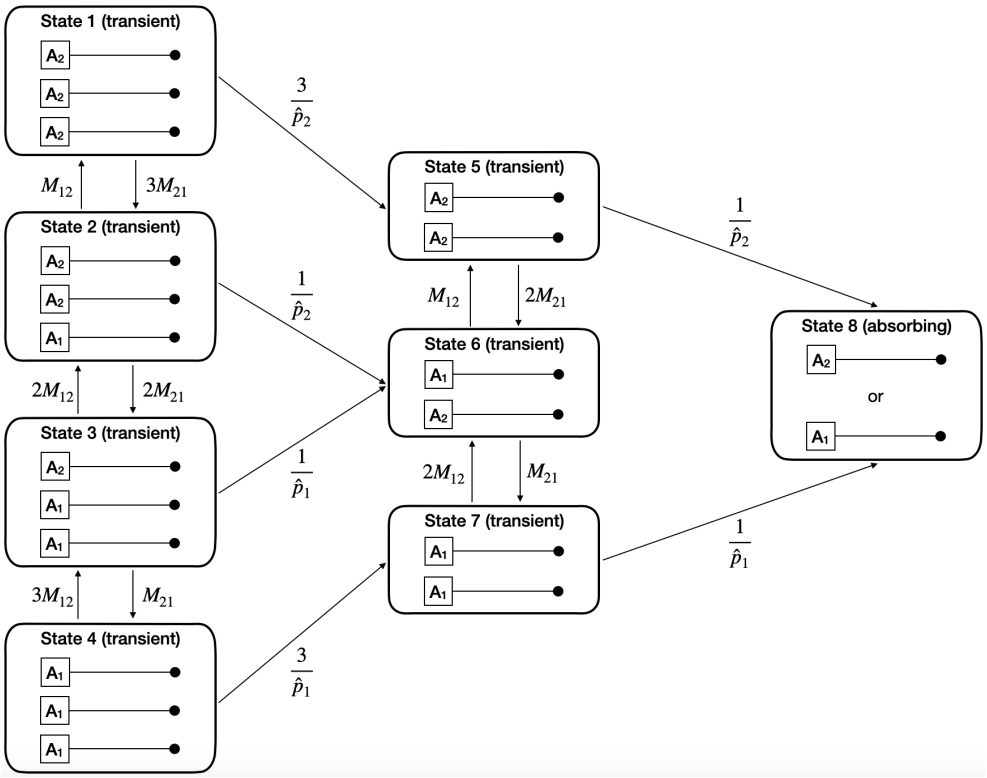

Figure S4: Transition rates between the states of the equilibrium balancing selection model for a sample of size three. Time is scaled in units of $2N_e$ generations. The neutral locus is represented by a black dot.

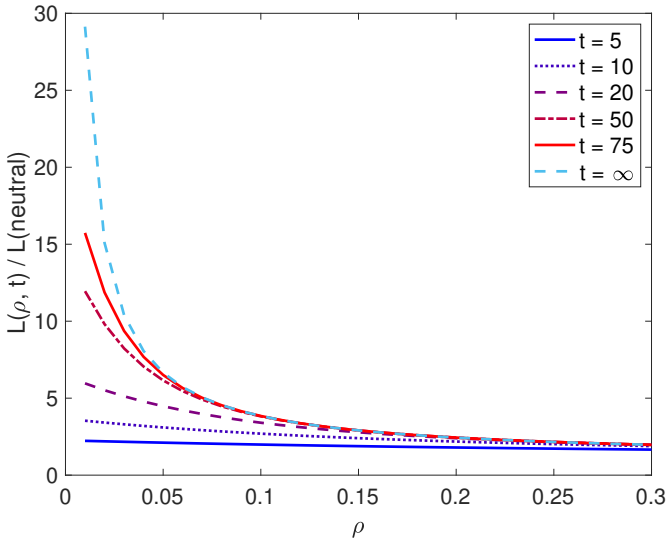

(a)

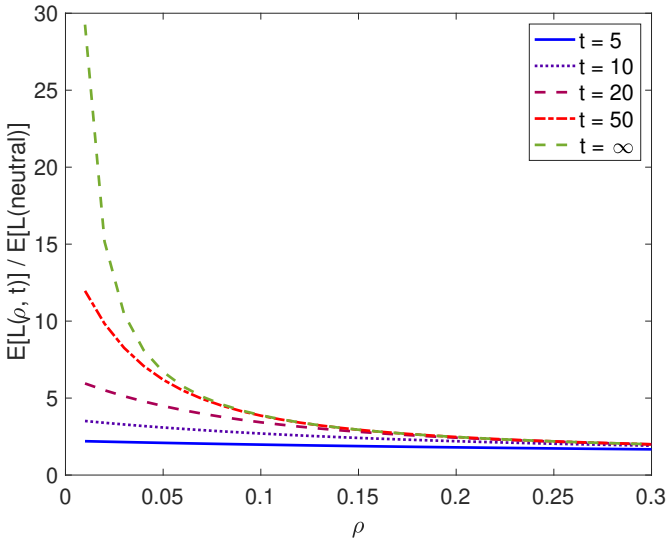

(b)

Figure S5: The approach to equilibrium diversity level. The parameters are the same as those used in Figures 6 and 8. The sample size is 20. $\hat{p}_2 = 0.75$ in (a) and 0.5 in (b). Note that the curves are based on a model without reversible mutation between the two selected variants A_1 and A_2. They overestimate the increase in diversity when ρ is very small.

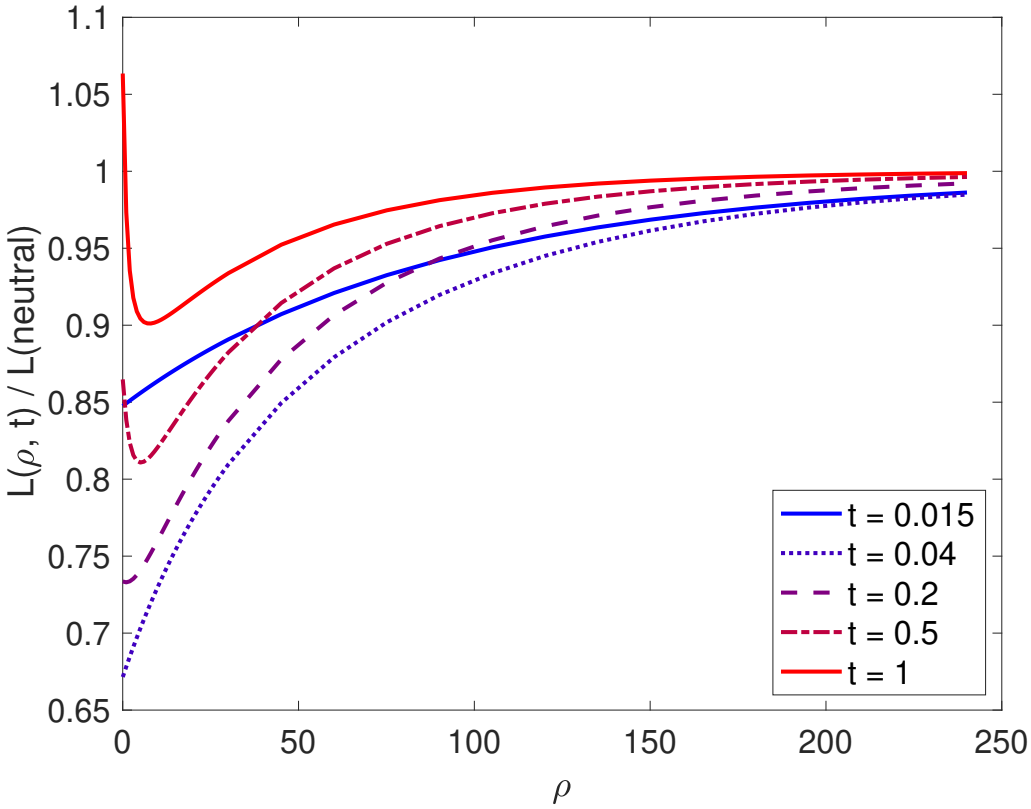

Figure S6: Neutral diversity in genomic regions surrounding a recently-emerged variant under balancing selection. The parameters are the same as in Figure 8 in the main text, except that the sample size is $n = 20$.

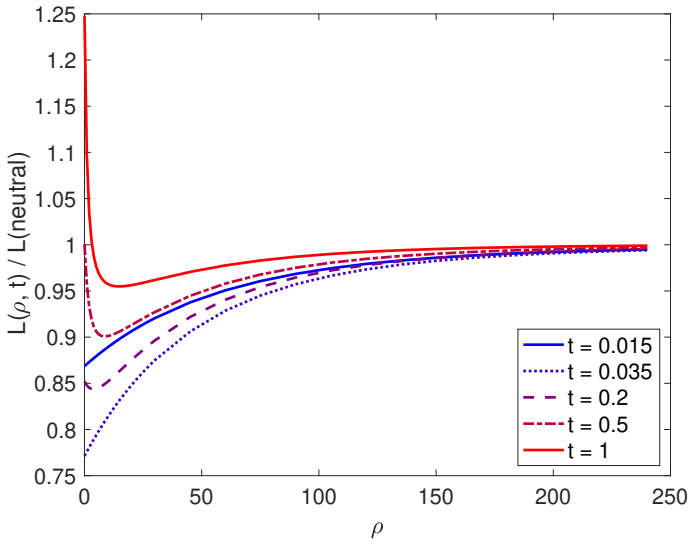

(a)

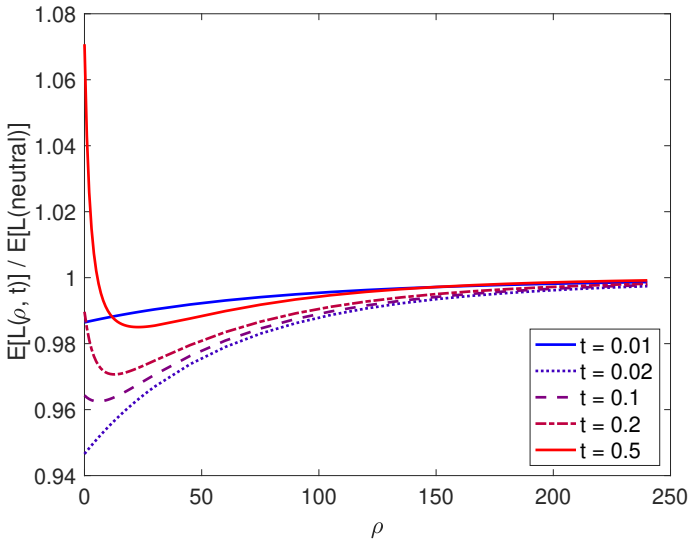

(b)

Figure S7: Neutral diversity level in genomic regions surrounding a recently-emerged balanced polymorphism. These figures are analogous to that in Figure 8, except that in (a) $\hat{p}_2 = 0.5$ and in (b) $\hat{p}_2 = 0.25$. The sample size is two.

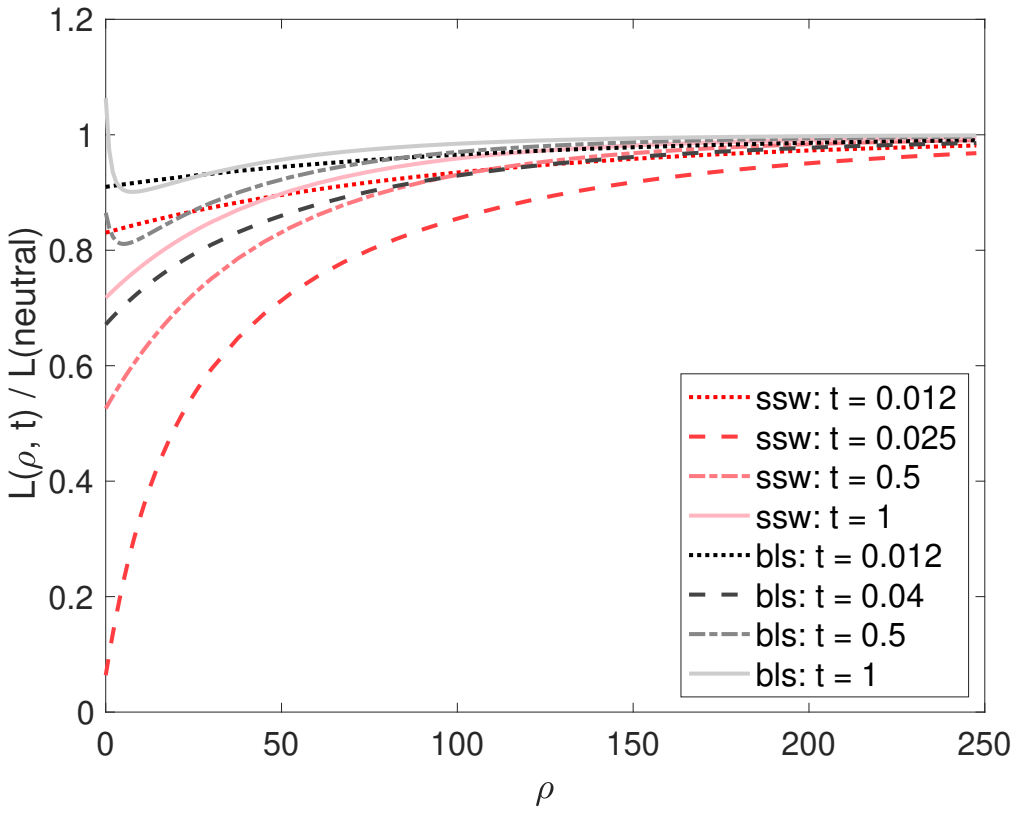

Figure S8: Comparing recent balancing selection with the corresponding sweep model with respect to their effects on diversity levels in surrounding genomic regions. The models and their parameters are the same as those in Figure 9, expect that $n = 20$.

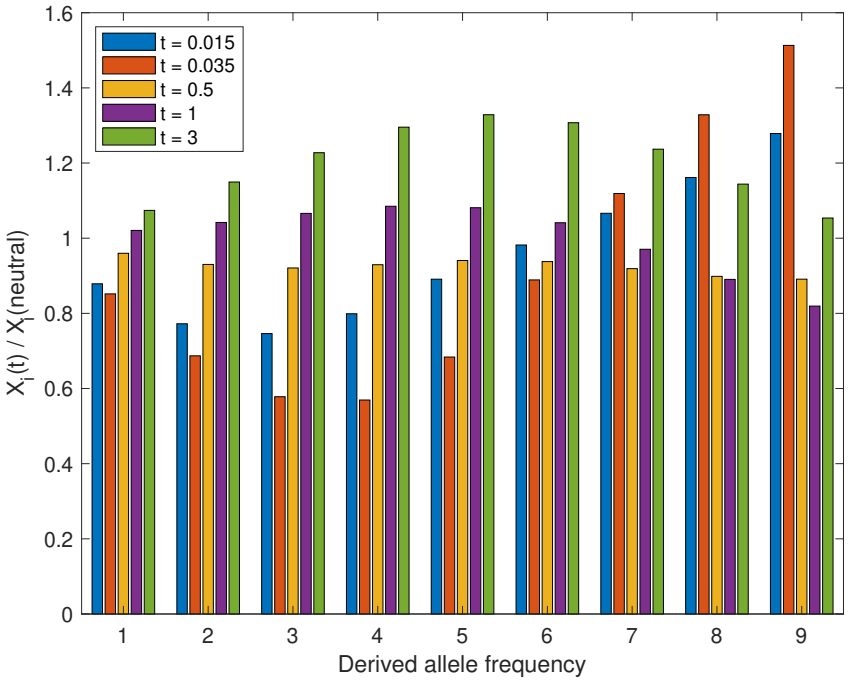

(a)

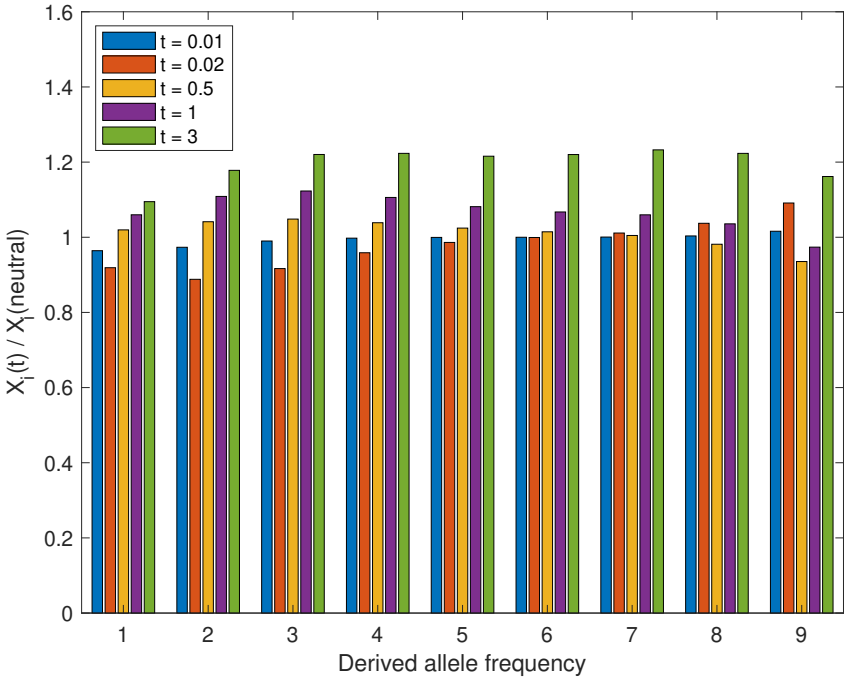

(b)

Figure S9: The SFS for the balancing selection models considered in Figure S7. In (a) $\hat{p}_2 = 0.5$ and in (b) $\hat{p}_2 = 0.25$.

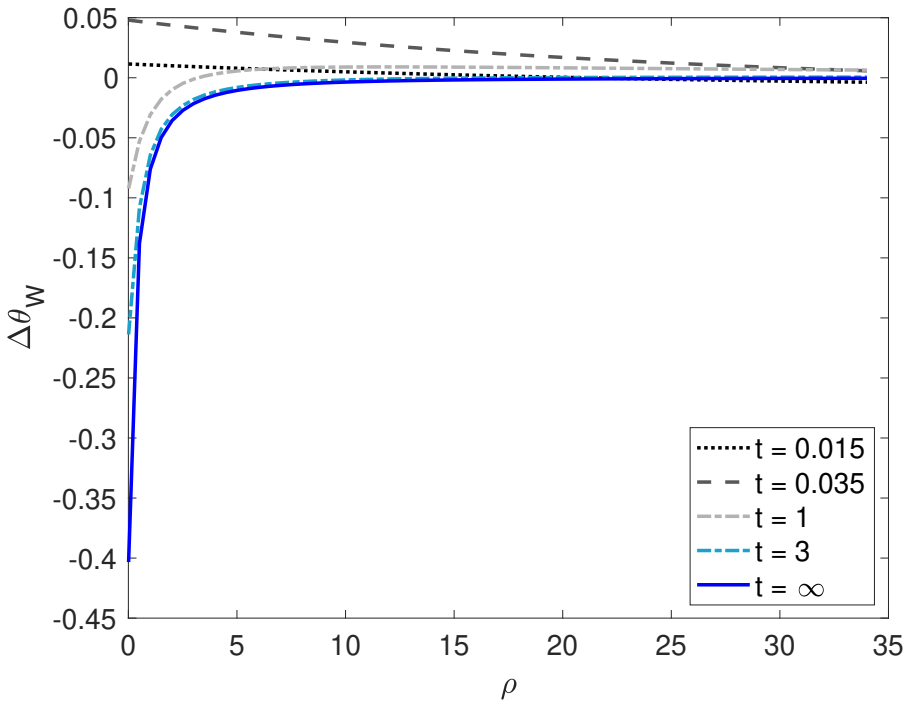

(a)

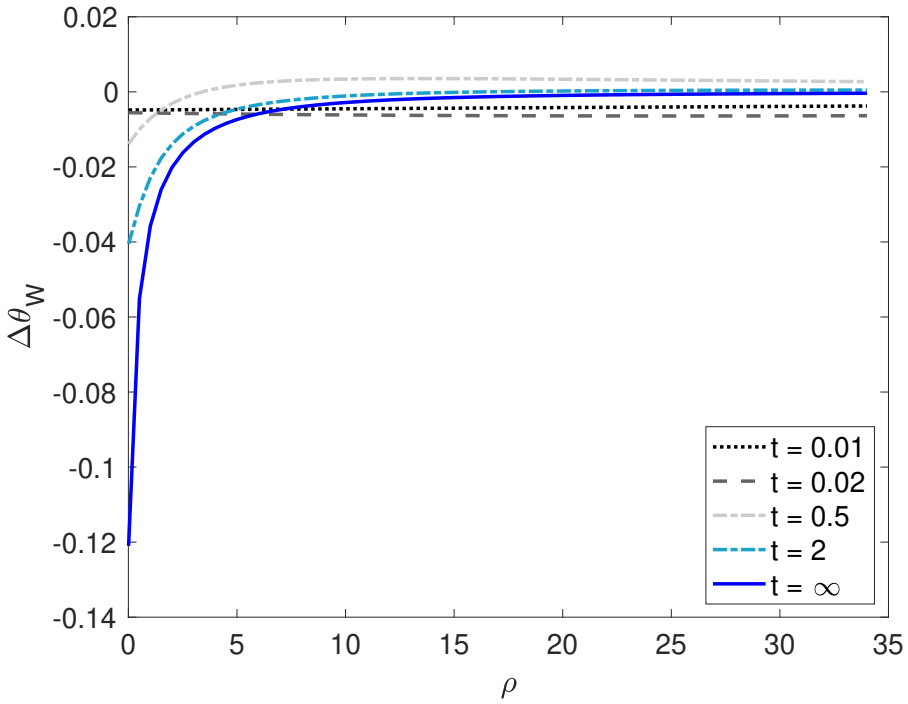

(b)

Figure S10: $\Delta\theta_W$ as a function of ρ and t for the balancing selection models considered in Figure S7. The sample size is 10. In (a) $\hat{p}_2 = 0.5$ and in (b) $\hat{p}_2 = 0.25$.